

# The 1000 Brightest HIPASS Galaxies: H I Properties

B. S. Koribalski<sup>1</sup>, L. Staveley-Smith<sup>1</sup>, V. A. Kilborn<sup>1,2</sup>, S. D. Ryder<sup>3</sup>, R. C. Kraan-Korteweg<sup>4</sup>, E. V. Ryan-Weber<sup>5,1</sup>, R. D. Ekers<sup>1</sup>, H. Jerjen<sup>6</sup>, P. A. Henning<sup>7</sup>, M. E. Putman<sup>8</sup>, M. A. Zwaan<sup>5,9</sup>, W. J. G. de Blok<sup>10,1</sup>, M. R. Calabretta<sup>1</sup>, M. J. Disney<sup>10</sup>, R. F. Minchin<sup>10</sup>, R. Bhathal<sup>11</sup>, P. J. Boyce<sup>10</sup>, M. J. Drinkwater<sup>12</sup>, K. C. Freeman<sup>6</sup>, B. K. Gibson<sup>2</sup>, A. J. Green<sup>13</sup>, R. F. Haynes<sup>1</sup>, S. Juraszek<sup>13</sup>, M. J. Kesteven<sup>1</sup>, P. M. Knezek<sup>14</sup>, S. Mader<sup>1</sup>, M. Marquarding<sup>1</sup>, M. Meyer<sup>5</sup>, J. R. Mould<sup>15</sup>, T. Oosterloo<sup>16</sup>, J. O'Brien<sup>6,1</sup>, R. M. Price<sup>7</sup>, E. M. Sadler<sup>13</sup>, A. Schröder<sup>17</sup>, I. M. Stewart<sup>17</sup>, F. Stootman<sup>11</sup>, M. Waugh<sup>5,1</sup>, B. E. Warren<sup>6,1</sup>, R. L. Webster<sup>5</sup>, and A. E. Wright<sup>1</sup>

## ABSTRACT

We present the HIPASS Bright Galaxy Catalog (BGC) which contains the 1000 H I-brightest galaxies in the southern sky as obtained from the H I Parkes All-Sky Survey (HIPASS). The selection of the brightest sources is based on their H I peak flux density ( $S_{\text{peak}} \gtrsim 116$  mJy) as measured from the spatially integrated HIPASS spectrum. The derived H I masses range from  $\sim 10^7$  to  $4 \times 10^{10} M_{\odot}$ . While the BGC ( $z < 0.03$ ) is complete in  $S_{\text{peak}}$ , only a subset of  $\sim 500$  sources can be considered complete in integrated H I flux density ( $F_{\text{HI}} \gtrsim 25$  Jy km s<sup>-1</sup>).

The HIPASS BGC contains a total of 158 new redshifts. These belong to 91 new sources for which no optical or infrared counterparts have previously been cataloged, an additional 51 galaxies for which no redshifts were previously known, and 16 galaxies for which the cataloged optical velocities disagree. Of the 91 newly cataloged BGC sources, only four are definite H I clouds: while three are likely Magellanic debris with velocities around 400 km s<sup>-1</sup>, one is a tidal cloud associated with the NGC 2442 galaxy group. The remaining 87 *new* BGC sources, the majority of which lie in the Zone of Avoidance, appear to be galaxies. We identified optical counterparts to all but one of the 30 *new* galaxies at Galactic latitudes  $|b| > 10^{\circ}$ . Therefore, the BGC yields no evidence for a population of "free-floating" intergalactic H I clouds without associated optical counterparts.

HIPASS provides a clear view of the local large-scale structure. The dominant features in the sky distribution of the BGC are the Supergalactic Plane and the Local Void. In addition, one can clearly see the Centaurus Wall which connects via the Hydra and Antlia clusters to the Puppis filament. Some previously hardly noticed galaxy groups stand out quite distinctively in the H I sky distribution. Several new structures are seen for the first time, not only behind the Milky Way.

*Subject headings:* surveys — galaxies: distances and redshifts, fundamental parameters, kinematics and dynamics — intergalactic medium — radio emission lines

<sup>1</sup>Australia Telescope National Facility, CSIRO, P.O. Box 76, Epping, NSW 1710, Australia.

<sup>2</sup>Centre for Astrophysics and Supercomputing, Swinburne University of Technology, P.O. Box 218, Hawthorn, VIC 3122, Australia.

<sup>3</sup>Anglo-Australian Observatory, P.O. Box 296, Epping, NSW 1710, Australia.

<sup>4</sup>Departamento de Astronomía, Universidad de Guanajuato,

juato, Apartado Postal 144, Guanajuato, Gto 36000, Mexico.

<sup>5</sup>School of Physics, University of Melbourne, VIC 3010, Australia.

<sup>6</sup>Research School of Astronomy & Astrophysics, Mount Stromlo Observatory, Cotter Road, Weston, ACT 2611, Australia.

<sup>7</sup>Institute for Astrophysics, University of New Mexico,

## 1. Introduction

Neutral hydrogen (HI) is a major component of the interstellar medium (ISM) in galaxies. The ISM provides fuel for the initial formation of molecular clouds and stars, and conversely acts as a reservoir for recycled gas from stars and supernovae. The total HI content of galaxies at a given epoch provides important constraints on the evolution of galaxies (Pei, Fall & Hauser 1999). At high redshifts, HI content is commonly estimated through observations of the damped Lyman- $\alpha$  (DLA) absorption-line systems (Rao & Turnshek 2000; Storrie-Lombardi & Wolfe 2000; Turnshek & Rao 2002). These observations appear to indicate that the HI density of the Universe is substantially higher at redshift  $z \approx 1 - 3$  compared to the  $z = 0$  density measured from 21-cm observations of optically-selected galaxy samples (e.g. Rao & Briggs 1993). However, there are large uncertainties in the interpretation of DLA statistics at high redshift because of lensing and dust obscuration. There are also uncertainties at low redshifts because our knowledge of HI in galaxies is heavily biased towards optically-selected samples. Are there, for example, many gas-rich galaxies or intergalactic clouds missing from the nearby galaxy census as some absorption-line observations of low column density systems ( $10^{12.5} - 10^{15.5} \text{ cm}^{-2}$ ) appear to indicate (Penton, Shull & Stocke 2000;

McLin et al. 2002; Ellison et al. 2002)?

Within individual galaxies, HI is frequently found to extend well outside the stellar radius (e.g. Broeils & van Woerden 1994; Meurer et al. 1996; Salpeter & Hoffman 1996; Broeils & Rhee 1997). Between galaxies neutral hydrogen is found mostly in the form of tidal tails, bridges and rings (Hibbard & van Gorkom 1996; Duc & Mirabel 1997; Hibbard et al. 2001; Ryder et al. 2001; Koribalski & Dickey 2004), which trace the interaction history of galaxies. Out of tidal HI debris, which constitute part of the intergalactic medium, new galaxies can form. These are known as ‘tidal-dwarf galaxies’ because of their similarity to classical dwarf irregulars and blue compact dwarf galaxies (Barnes & Hernquist 1992; Duc & Mirabel 1998; Duc et al. 2000; Hibbard et al. 2001; Braine et al. 2001). The closest and most prominent interacting galaxies are, of course, the Magellanic Clouds, which are associated with a range of extended tidal HI features, most prominently the Magellanic Bridge between the LMC and SMC, the Magellanic Stream (Mathewson, Cleary & Murray 1974) and the recently discovered Leading Arm (Putman et al. 1998; Putman et al. 2003). Other HI structures such as the Leo ring (Schneider 1989) and the tidal HI remnant known as the Virgo cloud (Giovanelli & Haynes 1989; Chengalur et al. 1995) have been discovered by accident and indicate the potential for new discoveries in blind HI surveys.

The HI content of normal galaxies varies strongly, depending on morphological type, optical diameter and the environment (Roberts & Haynes 1994; Haynes, Giovanelli & Chincarini 1984; Giovanelli & Haynes 1990; Solanes, Giovanelli & Haynes 1996; Solanes et al. 2001; Verdes-Montenegro et al. 2001). Whereas early-type galaxies tend to be gas-poor (Duprie & Schneider 1996; Sadler 2001; Oosterloo et al. 2002), late-type galaxies are typically gas-rich (Matthews, Gallagher & Littleton 1995; Solanes et al. 2001). HI can also be easily detected in many low surface-brightness (LSB) and late-type dwarf galaxies, often barely visible in the optical (e.g., Impey & Bothun 1997). Therefore, blind HI surveys will reveal classes of galaxies that are under-represented in optical surveys. Since galaxy clustering is known to decrease from early- to late-type galaxies (Giuricin et al. 2001) this will affect our overall

---

800 Yale Blvd, NE, Albuquerque, NM 87131, USA.

<sup>8</sup>CASA, University of Colorado, Boulder, CO 80309-0389, USA

<sup>9</sup>European Southern Observatory, Karl-Schwarzschild-Str. 2, D-85748 Garching bei Muenchen, Germany

<sup>10</sup>Cardiff School of Physics & Astronomy, Cardiff University, 5 The Parade, Cardiff, CF24 3YB, U.K.

<sup>11</sup>Department of Physics, University of Western Sydney Macarthur, P.O. Box 555, Campbelltown, NSW 2560, Australia.

<sup>12</sup>Department of Physics, University of Queensland, QLD 4072, Australia.

<sup>13</sup>School of Physics, University of Sydney, NSW 2006, Australia.

<sup>14</sup>WIYN, Inc. 950 North Cherry Avenue Tucson, AZ 85726, USA.

<sup>15</sup>National Optical Astronomy Observatories, P.O. Box 26732, 950 North Cherry Avenue, Tucson, AZ, USA.

<sup>16</sup>ASTRON, P.O. Box 2, 7990 AA Dwingeloo, The Netherlands.

<sup>17</sup>Department of Physics & Astronomy, University of Leicester, Leicester LE1 7RH, U.K.

view of the local large-scale structure.

The galaxy distribution in the nearby Universe reveals many coherent structures (Geller & Huchra 1989; Fairall et al. 1990; Fairall 1998), such as the Supergalactic Plane (SGP), the Fornax and Centaurus Walls, as well as the Local Void (to name the most prominent in the southern sky). Since our knowledge about the local large-scale structure has, so far, mostly been determined by extensive optical and infrared surveys of the sky (e.g. Lauberts 1982, Jarrett et al. 2003), not much is known about the connectivity of structures across the artificial gap created by the extinction of dust in our own Galaxy. This can affect up to  $\sim 25\%$  of the sky (e.g. Kraan-Korteweg & Lahav 2000) and obscures our view of important regions such as the putative Great Attractor (Lynden-Bell et al. 1988). However, 21-cm observations are unaffected by dust extinction, so are easily able to complement optical and infrared galaxy surveys and substantially improve the census of galaxies and the measurement of the baryon content of the local Universe.

### 1.1. H I Surveys

Many H I surveys have been targeted at cataloged galaxies, galaxy groups, clusters and selected regions — for a summary see Salzer & Haynes (1996) or Zwaan et al. (1997). The biggest targeted H I surveys to-date are those by (a) Fisher & Tully (1981a) who obtained H I spectra for 1171 galaxies (out of 1787 targets) with the NRAO 91-m and 43-m telescopes and the Bonn 100-m telescope, (b) Schneider et al. (1990) who obtained H I spectra for 762 dwarf and other LSB galaxies with the Arecibo telescope, (c) Mathewson, Ford, & Buchhorn (1992; hereafter MFB92) who obtained H I spectra for 551 galaxies with the Parkes telescope, (d) Haynes et al. (1997) who obtained H I spectra for about 500 galaxies in 27 Abell clusters visible from Arecibo, (e) Theureau et al. (1998) who present 2112 H I spectra of cataloged spiral galaxies obtained with the Nançay radiotelescope, and (f) Haynes et al. (1999) who obtained H I spectra for 881 galaxies, over 500 of which were detected with the 91-m Green Bank telescope.

Overall, there are currently about three times more H I measurements in the northern hemisphere ( $\gtrsim 10300$ ) than in the south ( $\gtrsim 3500$ ), as determined from the Lyon/Meudon Extragalactic

Database (LEDA). At declinations south of  $-45^\circ$  ( $\sim 30\%$  of the southern sky) only 560 H I measurements are available. The most prominent (targeted) southern H I catalog is that by MFB92 who published H I profiles for 551 galaxies of type Sb to Sd. Earlier, Reif et al. (1982) and Longmore et al. (1982) successfully obtained 196 and 100 H I profiles, respectively, with the Parkes telescope, and Fouqué et al. (1990a) published H I profiles of 242 southern late-type galaxies in the declination range  $-38^\circ$  to  $-17^\circ$  obtained with the Nançay telescope.

One of the earliest *blind* H I surveys was that by Kerr & Henning (1987) who detected 16 previously uncataloged galaxies in the Zone of Avoidance (ZOA) and considered the possibility of future whole sky surveys with multibeam instruments (see also Henning 1995). Schneider (1996) gives a summary of other blind H I survey programs. Until recently, the Arecibo Dual-Beam Survey (ADBS) and the deeper Arecibo H I strip survey (AHISS, see Zwaan et al. 1997) were the largest blind 21-cm surveys (see Table 1) carried out, covering areas of 430 and 65 square degrees, respectively. With the advent of a 21-cm multibeam system at the 64-m Parkes telescope (Staveley-Smith et al. 1996) as well as new observing and data reduction software (Barnes et al. 2001), much larger and deeper surveys are now possible. For example, Henning et al. (2000) did a shallow survey of 1800 square degrees of sky in the southern Zone of Avoidance, finding 110 H I sources, 67 of which had no previously published optical counterpart.

This paper is organized as follows: the observations and data reduction are described in Section 2, followed by a detailed description of the ‘HIPASS Bright Galaxy Catalog’ in Section 3. The H I properties from the BGC are discussed in Section 4, followed by a study of the large-scale structure in Section 5. Our conclusions are given in Section 6.

In related papers: Ryan-Weber et al. (2002) study 138 galaxies from the BGC which had no redshift measurements prior to the commencement of the H I multibeam surveys. Zwaan et al. (2003) analyze the BGC completeness and derive a new H I mass function.

## 2. HIPASS Observations & Data Reduction

The observations utilized the 21-cm multibeam receiver (Staveley-Smith et al. 1996) installed at the prime focus of the Parkes<sup>18</sup> 64-m radio telescope. The receiver has thirteen beams, each with two linear polarizations, and system temperatures of around 20 K. The correlator has a bandwidth of 64 MHz divided into 1024 channels, covering a velocity range of  $-1200 < cz < +12700$  km s<sup>-1</sup>, at a channel spacing of 13.2 km s<sup>-1</sup>. The velocity resolution, after Tukey 25% smoothing (Barnes et al. 2001) is 18 km s<sup>-1</sup>. Data for HIPASS was gathered by scanning the telescope across the sky in 8° strips in Declination ( $\delta$ ). Five sets of independent scans were made of each region, resulting in a final sensitivity of  $\sim 40$  mJy beam<sup>-1</sup> ( $3\sigma$ ) per channel. Assuming a velocity width of 100 km s<sup>-1</sup> the theoretical  $5\sigma$  HI column density of HIPASS is  $3 \times 10^{18}$  cm<sup>-2</sup> (only applicable for very extended objects filling the beam). Observations were conducted from 1997 to 2000, and the whole of the southern sky ( $\delta < +2^\circ$ ) was covered. Note that the HIPASS BGC (see Section 3) only includes sources with  $\delta < 0^\circ$ . Observations for the northern extension to HIPASS ( $+2^\circ < \delta < +25^\circ$ ) and for the Jodrell Bank HIJASS survey ( $\delta > +22^\circ$ ) will be reported elsewhere (see, e.g., Boyce et al. 2001, Lang et al. 2003).

The data was bandpass corrected, calibrated and Doppler-tracked using the AIPS++ program LIVE DATA and then gridded with GRIDZILLA into 388 slightly overlapping cubes of size  $8^\circ \times 8^\circ$ , and pixel size  $4'$ . The mean Parkes beam is  $14'3$ , but the gridding process slightly degrades the angular resolution. Moreover, the beam varies slightly with source strength and extent (see Barnes et al. 2001). For the HI parameterization (see Section 3.3) we use a beam size of  $15'5$ . All velocities are in the usual ‘optical’ convention ( $v = cz$ ) and heliocentric reference frame. Continuum ripple, proportional in amplitude to the detected 20-cm continuum emission, was removed using a ‘scaled template method’, though some residual ripple at the position of strong radio continuum sources (e.g. the nearby Centaurus A galaxy, see Sec-

tion 3.6) still remains. HIPASS spectra, smoothed spatially to a pixel size of  $8'$ , are available at [www.atnf.csiro.au/research/multibeam/](http://www.atnf.csiro.au/research/multibeam/). The HI spectra of all 1000 HIPASS BGC sources are displayed in Fig. 1 (see Section 3).

### 2.1. Flux Calibration

The absolute flux calibration of HIPASS (see Barnes et al. 2001) is based on the 20-cm flux density of the extragalactic radio sources PKS 1934–638 (14.9 Jy at 1420 MHz) and Hydra A (40.6 Jy at 1395 MHz). Whereas PKS 1934–638 is a compact source, unresolved with the Parkes telescope, Hydra A is an extended radio galaxy (diameter  $\sim 8'$ , Taylor et al. 1990; Lane et al. 2004) with a total flux density of 43.2 Jy at 1395 MHz (Baars et al. 1977). To account for beam dilution the flux density of Hydra A is reduced by  $\sim 6\%$  (J. Reynolds, priv. comm.) for the HIPASS calibration.

For comparison, MFB92 for their absolute flux calibration use Hydra A with a flux density of 43.5 Jy at 1410 MHz (no correction for beam dilution was applied) and the galaxy IC 4824 with an integrated HI flux density of 20.0 Jy km s<sup>-1</sup>. We measure  $F_{\text{HI}} = 17.0 \pm 2.7$  Jy km s<sup>-1</sup> for IC 4824 (HIPASS J1913–62), slightly lower than the value used by MFB92 and consistent with the difference in absolute flux calibration. See Section 4.4 for a comparison of the BGC  $F_{\text{HI}}$  measurements with other HI surveys.

## 3. The HIPASS Bright Galaxy Catalog

A catalog of the 1000 HI-brightest galaxies was compiled using HIPASS data from the whole southern sky ( $\delta < 0^\circ$ ). Throughout this paper we refer to this catalog as the HIPASS Bright Galaxy Catalog (BGC). The galaxy finding, selection criteria, optical identification and HI parameterization are described in detail in the following subsections. The HI spectra of all 1000 BGC sources are displayed in Fig. 1 and the HI properties together with their optical (or in some cases infrared) identifications, where available, are given in Table 2. For a description of the table columns see Section 3.4. The full versions of Fig. 1 and Table 2 are in the electronic edition of the Journal, while the printed edition contains only a sample. The HIPASS BGC and additional information is available at

<sup>18</sup>The Parkes telescope is part of the Australia Telescope which is funded by the Commonwealth of Australia for operation as a National Facility managed by CSIRO.

[www.atnf.csiro.au/research/multibeam/](http://www.atnf.csiro.au/research/multibeam/).

The HIPASS BGC overlaps with recently published HI catalogs of particular regions of the sky based on the same set of data: Banks et al. (1999; the nearby Centaurus A Group); Putman et al. (2002; HVC catalog, including some nearby galaxies); Kilborn et al. (2002; South Celestial Cap) and Waugh et al. (2002; Fornax region). Although the HI parameters of a HIPASS source can vary slightly between catalogs, depending on the chosen fitting parameters, the HIPASS name of each source (e.g. HIPASS J1712-64) is maintained for consistency and cross-identification purposes. Following standard nomenclature, letters ('A', 'B', etc.) are appended to a name where the positions are similar enough that two or more sources would have the same name.

The HIPASS BGC also overlaps with the HIPASS Catalogue (HICAT: Meyer et al. 2004, Zwaan et al. 2004) which contains 4315 HI sources with systemic velocities between  $\sim 300$  and  $12700 \text{ km s}^{-1}$  (see Table 1). Optical identification of the HICAT sources is under way. Note that HICAT and the BGC are based on the same survey data, but were compiled and parameterized independently.

### 3.1. Galaxy Finding

An automatic galaxy-finding algorithm, MULTIFIND (Kilborn 2001; Kilborn et al. 2002), was run on the 388 edge-masked HIPASS cubes covering the whole southern sky, over all 1024 channels (i.e.  $-1200$  to  $+12700 \text{ km s}^{-1}$ ), with an HI peak flux density cutoff of  $60 \text{ mJy beam}^{-1}$ . The resulting source list is very large because the algorithm is designed to detect all signals above a certain strength when present over two or more consecutive channels. Beside HI emission from our own Galaxy and many other galaxies, it also contains Galactic recombination lines and HVCs as well as artifacts such as interference and residual continuum ripple. After applying the selection criteria (see below), each HI spectrum was inspected by eye to eliminate any artifacts as well as Galactic signals. In many cases the corresponding HIPASS cube was inspected to reliably classify the signal based on the surrounding pixels and neighbouring channels. For example, Galactic recombinations lines were rejected on the basis that they appear at several, well-defined frequencies (see Sec-

tion 3.7.1). Residual interference, where present, was rejected as it is usually narrow, intermittent and scattered over many degrees.

### 3.2. Selection Criteria

From the extensive source list we extracted a galaxy candidate list with systemic velocity  $v_{\text{sys}} = -1200$  to  $8000 \text{ km s}^{-1}$  (excluding  $\pm 350 \text{ km s}^{-1}$ ), and Galactic latitude  $|b| > 3^\circ$ . The range  $|v| < 350 \text{ km s}^{-1}$  was omitted in the selection because of confusion with HVCs (see Putman et al. 2002) which makes it difficult to identify galaxies at those velocities. The latitude range of  $|b| < 3^\circ$  was omitted due to contamination by extensive continuum ripple from Galactic sources and therefore particularly difficult for an automatic galaxy finder. This was possible because this area had already been searched extensively by eye using the Parkes HI ZOA shallow survey (HIZSS; Henning et al. 2000) which was conducted contemporaneously with HIPASS. To overcome the velocity and latitude gaps we added to our galaxy candidate list the positions of all known galaxies with systemic velocities  $v_{\text{sys}} < 350 \text{ km s}^{-1}$  (using the NASA/IPAC Extragalactic Database, NED) as well as galaxies from the HIZSS ( $|b| < 5^\circ$ ). All galaxies are then parameterized using HIPASS data.

### 3.3. HI Parameterization

The HI parameterization is carried out semi-automatically using several MIRIAD programs. For each source, the HI emission profile was inspected using preliminary positions and velocities as obtained from MULTIFIND or, in case of the added sources (see above), from the HIZSS and NED. If necessary, the velocities were adjusted, and an integrated HI intensity map produced (program MOMENT). This, in turn, was used to estimate the HI centroid using a Gaussian fit (program IMFIT). The fitting area (a polygon) was set manually according to the source size. Based on the measured centroid, a weighted spectrum was then formed. To this spectrum, a first-order baseline was fit and subtracted (see Fig. 1). The HI peak and integrated flux densities, the systemic velocity and the velocity widths were then measured (program MBSPECT).

Most galaxies are point sources in HIPASS; i.e.

their intrinsic size is much smaller than the  $15''.5$  angular resolution of the gridded data. For these sources we considered data in a region of size  $20' \times 20'$ , centered on each source, and weighted each pixel according to the expected beam response. To find extended sources, we also directly summed the flux in a region of size  $28' \times 28'$ . Sources with at least 10% more flux were flagged as potentially extended, and the cube was manually inspected. Where the increased flux was due to confusion with a neighbouring galaxy, the point source model was used and the galaxy marked as confused (c). Truly extended galaxies (marked with "e") were re-parameterized using MBSPECT with a more appropriate box size (see Section 4.2).

Altogether, more than 8000 spectra ( $\sim 70\%$  of which were multiple entries) were inspected. Galactic signals (e.g. recombination lines) as well as artifacts (interference, continuum ripple, etc.) were removed or cataloged separately (e.g. HVCs; see Putman et al. 2002). Of the 1400 galaxies finally parameterized, 1000 have HI peak flux densities  $\gtrsim 116$  mJy. Assuming a velocity width of  $100 \text{ km s}^{-1}$  this corresponds to a column density limit of  $\sim 10^{19} \text{ cm}^{-2}$  (for objects filling the beam) and an HI mass limit of  $2 \times 10^6 \times D^2 M_{\odot}$ , where  $D$  is the galaxy distance in Mpc.

The Large Magellanic Cloud (LMC) and the Small Magellanic Cloud (SMC) obey the BGC selection criteria. However, their huge angular sizes make it difficult to parameterize their HI properties in the same way as the BGC sources. Their HI parameters have therefore been obtained from separate Parkes observations and are not included in Table 2 (or any of the discussions). Both the standard HIPASS reduction technique, and the modified MINMED5 method used by Putman et al. (2003) substantially underestimate the integrated HI flux density in the Magellanic Clouds. Staveley-Smith et al. (2003) measure an integrated HI flux density of  $8.1 \times 10^5 \text{ Jy km s}^{-1}$  for the LMC. Adopting a distance of 50 kpc this gives an HI mass of  $4.8 \times 10^8 M_{\odot}$ . Stanimirovic et al. (1999) measure an integrated HI flux density of  $4.5 \times 10^5 \text{ Jy km s}^{-1}$  for the SMC. Adopting a distance of 60 kpc this gives an HI mass of  $3.8 \times 10^8 M_{\odot}$ . We refer to Westerlund (1997) for a detailed discussion of the Magellanic Cloud distances.

### 3.4. The HI Data

Fig. 1 shows the integrated HI spectra for all 1000 BGC sources (only two example pages are given in the printed version of the journal; all HI spectra are given in the electronic version). Marked in each HIPASS spectrum are several measured HI parameters (the peak flux density, 50% and 20% velocity widths) as well as the velocity range over which the HI emission profile is parameterized. The velocity range displayed outside the profile was used for the first order baseline fit. The width-maximized 50% and 20% points are highlighted with a circle and the width-minimized points are highlighted with a cross (in most cases these fall on the same positions due to the chosen velocity range).

The HI properties obtained for all 1000 HIPASS BGC sources are listed in Table 2. The columns are as follows:

- *Col. (1)* HIPASS name,
- *Cols. (2+3)* fitted HI position in RA, DEC (J2000),
- *Cols. (4+5)* Galactic longitude,  $l$ , and latitude,  $b$ , in degrees,
- *Col. (6)* most likely optical (or infrared) identification(s) (see Section 3.5),
- *Col. (7+8)* the HI peak flux density,  $S_{\text{peak}}$ , and its uncertainty,  $\sigma(S_{\text{peak}})$ , in Jy, (spatially integrated, where appropriate)
- *Col. (9+10)* the integrated (spatially and spectrally) HI flux density,  $F_{\text{HI}}$ , and its uncertainty,  $\sigma(F_{\text{HI}})$ , in  $\text{Jy km s}^{-1}$ ,
- *Col. (11+12)* the HI systemic velocity,  $v_{\text{sys}}$ , measured at the midpoint of the 50% level of the peak flux density, and its uncertainty,  $\sigma(v_{\text{sys}})$ , in  $\text{km s}^{-1}$ , (all velocities are in the heliocentric velocity frame using the optical convention),
- *Col. (13)* velocity line widths,  $w_{50}$ , in  $\text{km s}^{-1}$ , measured at the 50% level of the peak flux density (the uncertainty,  $\sigma(w_{50})$ , is about  $2 \times \sigma(v_{\text{sys}})$ , see Col. 12),
- *Col. (14)* velocity line widths,  $w_{20}$ , in  $\text{km s}^{-1}$ , measured at the 20% level of the peak flux density (the uncertainty,  $\sigma(w_{20})$ , is about  $3 \times \sigma(v_{\text{sys}})$ , see Col. 12),
- *Col. (15)* the Local Group velocity,  $v_{\text{LG}}$ , in  $\text{km s}^{-1}$ , calculated using  $v_{\text{LG}} = v_{\text{sys}} + 300 \sin l \cos b$ , and
- *Col. (16)* the logarithm of the HI mass,  $M_{\text{HI}}$ , calculated using  $M_{\text{HI}} [M_{\odot}] = 2.36 \times 10^5 D^2 F_{\text{HI}}$ ,

where  $F_{\text{HI}}$  is the integrated HI flux density in  $\text{Jy km s}^{-1}$ , and  $D$  the distance in Mpc. Distances are derived using  $D = v_{\text{LG}} / H_0$ , except for nine galaxies (see Section 3.4.2 and Table 3) for which we use independent distances. The latter are marked with a star (\*) in this column. We adopt a Hubble constant of  $H_0 = 75 \text{ km s}^{-1} \text{ Mpc}^{-1}$ .

—*Col. (17)* gives flags noting extended (e) and confused (c) sources, galaxies with no previous velocity measurement (:), or potentially incorrect velocity measurements (w), baseline ripple (r), and Hanning smoothing (h). Galaxy pairs and groups are also marked as such.

Note that we use a first order baseline fit for all but three BGC sources (HIPASS J0037–22, J0930–35, and J1324–42). For the latter a severe baseline ripple was present, and had to be subtracted out by high-order polynomial fits. Hanning smoothing was applied to the spectrum of one galaxy, HIPASS J0403–01, (to reduce spectral ringing) before the velocity range of the HI emission could be determined.

#### 3.4.1. Uncertainties in the measured HI properties

In the following we analyze the uncertainties in the measured HI properties, some of which can be determined more accurately than others. Uncertainties in the peak and integrated flux densities,  $\sigma(S_{\text{peak}})$  and  $\sigma(F_{\text{HI}})$ , respectively, and the systemic velocity,  $\sigma(v_{\text{sys}})$ , are given for each BGC source (see Cols. 8, 10 and 12 in Table 2). Other uncertainties can be calculated from these values or are given more generally.

The positional accuracy of a HIPASS source can be calculated as the gridded beam (15'5) divided by the HI signal-to-noise ratio. Since BGC sources generally have signal-to-noise ratios  $\gtrsim 9$ , the positional uncertainty is expected to be smaller than 1'.7. By comparing the HI positions given in Table 2 with those of the corresponding cataloged, optical or infrared counterparts (see Section 3.5) we find a standard deviation in RA, Dec of 1'.3.

The uncertainty in the peak flux density,  $\sigma(S_{\text{peak}})$ , of a HIPASS source is generally dominated by the r.m.s. noise in the corresponding HI spectrum. We measure an r.m.s. of  $\sim 13 \text{ mJy}$  for most of the survey. Increased noise levels are measured in the HI spectra of extended sources and in

regions of high 20-cm continuum flux density (see Section 2). In addition,  $\sigma(S_{\text{peak}})$  increases slightly with rising peak flux density (see Barnes et al. 2001); we estimate this as 5% of  $S_{\text{peak}}$ , resulting in  $\sigma(S_{\text{peak}})^2 = \text{rms}^2 + (0.05 S_{\text{peak}})^2$ . During the HI parametrisation of all BGC sources we measured the *clipped* r.m.s. (see Fig. 2), which is lower than the standard r.m.s. noise ( $\sigma_{\text{rms}}$ ). The clipped r.m.s. is calculated after five iterations of  $2\sigma$  clipping which is necessary to obtain a robust baseline fit in the line-free region of the HIPASS spectra.

There are various methods to estimate the uncertainty in the integrated flux density (see Reif et al. 1982, Schneider et al. 1990, Fouqué et al. 1990a). We use  $\sigma(F_{\text{HI}}) = 4 \times SN^{-1} (S_{\text{peak}} F_{\text{HI}} \delta v)^{1/2}$ , modified from the slightly more conservative estimate by Fouqué et al. (1990a). Here,  $SN$  is the ratio of  $S_{\text{peak}}$  to  $\sigma(S_{\text{peak}})$ , and  $\delta v = 18 \text{ km s}^{-1}$  is the velocity resolution of HIPASS. The mean  $F_{\text{HI}}$  uncertainty in the BGC is 15%  $F_{\text{HI}}$  ( $\sigma = 7\%$ ), although this is likely an overestimate (see Section 4.4).

The uncertainty in the systemic velocity is approximately  $\sigma(v_{\text{sys}}) = 3 \times SN^{-1} (P \delta v)^{1/2}$ . Again, we slightly modified the estimate by Fouqué et al. (1990a; see also Schneider et al. 1986, 1990). Here,  $P = 0.5 \times (w_{20} - w_{50})$  is a measure of the steepness of the profile edges. We find median values of  $P = 12 \text{ km s}^{-1}$  and  $\sigma(v_{\text{sys}}) = 4 \text{ km s}^{-1}$ .

Following Schneider et al. (1986) the uncertainties in the 50% and 20% velocity line widths are  $\sigma(w_{50}) = 2 \times \sigma(v_{\text{sys}})$  and  $\sigma(w_{20}) = 3 \times \sigma(v_{\text{sys}})$ , resulting in median values of  $8 \text{ km s}^{-1}$  and  $12 \text{ km s}^{-1}$ , respectively. The velocity widths listed in Table 2 have not been corrected for resolution and internal velocity dispersion (see, e.g., Tully & Fouqué 1985, Bottinelli et al. 1990, Fouqué et al. 1990b).

#### 3.4.2. Distances

For most BGC sources approximate distances are derived using  $D = v_{\text{LG}} / H_0$ , where  $v_{\text{LG}} = v_{\text{sys}} + 300 \sin l \cos b$  is the Local Group velocity and  $H_0 = 75 \text{ km s}^{-1} \text{ Mpc}^{-1}$ . Although independent distances are currently available for about 45 galaxies in the BGC (see Mateo 1998, Willick & Batra 2001, Karachentsev et al. 2003, and references therein) we adopted these only for the closest

galaxies ( $D < 2.2$  Mpc, see Table 3). We note that all but one of the galaxies with  $v_{\text{LG}} < 131 \text{ km s}^{-1}$  have independent distance estimates; the exception is the newly catalogued galaxy HIZSS 003 (HIPASS J0700–04) which has a Local Group velocity of  $115 \text{ km s}^{-1}$ . Fig. 3 shows distances versus HI Local Group velocities for all galaxies in the BGC with  $D \lesssim 5$  Mpc. For error bars on the independent distances (typically 10%) consult the above references.

### 3.5. Optical Identification

The search for optical (or infrared) counterparts was conducted using the NASA/IPAC Extragalactic Database (NED). For the identification we used both positional and velocity information. A search radius of  $6'$  was sufficient in most cases to find a cataloged galaxy, but because of the  $15'.5$  gridded beam, sources within that sky area and with similar velocities may contribute and confuse the HI emission spectrum and flux density measurement. The measured HI systemic velocity was used to identify the most likely optical counterpart(s), whenever previously cataloged velocities were available in NED. For further analysis, in particular to obtain the optical properties of galaxies in the BGC (presented in a forthcoming paper) we also used the Lyon/Meudon Extragalactic Database (LEDA). Figs. 4 and 5 show the separations between the fitted HI position, from HIPASS, and the optical positions for all 853 galaxies with single optical identifications in LEDA, i.e. galaxy pairs and groups as well as the newly cataloged galaxies and HI clouds are not included here. The difference between the measured HI systemic velocity of HIPASS BGC members and the optical velocities of their LEDA counterparts is shown in Fig. 6. The scatter diagram (Fig. 4) reveals no systematic offset of the positions at any peak flux density level. The standard deviation in RA and Dec is  $\sigma_{\text{RA}} = 1'.0$  and  $\sigma_{\text{DEC}} = 0'.8$ , respectively. Galaxy positions from HIPASS are therefore generally accurate to within a few arcminutes, with the actual value depending on the HI peak flux density and source extent (Barnes et al. 2001). Large offsets between the HI and the optical positions usually occur when multiple galaxies contribute to the signal or when the HI distribution is asymmetric or peculiar. It is likely that occasionally an optical galaxy has

been mis-identified as the counterpart to a BGC source, which might result in a relative large position offset. For example, we found one source, HIPASS J0622–07 ( $v_{\text{sys}} = 754 \text{ km s}^{-1}$ ), for which the proposed optical counterpart, CGMW1-0080, at a projected distance of  $5'.6$  is not the correct identification (see Fig. 7). HI follow-up observations with the Australia Telescope Compact Array (ATCA) revealed a previously uncataloged galaxy, less than  $1'$  from the HIPASS position and easily visible in the Digitized Sky Survey (the galaxy center is close to a star; see also Whiting, Hau & Irwin 2002).

For 91 sources, NED had no catalog entry, mainly because of Galactic extinction (see Section 4.1). Additionally, for 51 galaxies, no velocity information was recorded in NED (these are flagged with ‘.’ in Table 2). For 16 galaxies, the first-listed NED velocity differs significantly, mostly a result of some incorrect optical measurements; these are labeled ‘w’ (for details see Appendix A). At least 44 BGC sources correspond to galaxy pairs and 11 to compact galaxy groups. More than 68 galaxies are confused (‘c’) by a neighbouring galaxy. As a result their HI flux densities maybe slightly overestimated.

### 3.6. HI absorption

The HI spectra of the galaxies NGC 253 (HIPASS J0047–25), NGC 3256 (HIPASS J1028–43), NGC 4945 (HIPASS J1305–49), Circinus (HIPASS J1413–65), NGC 5128 (Centaurus A, HIPASS J1324–42) and possibly others are affected by HI absorption against their bright radio nuclei. The integrated HI flux density and HI mass of these galaxies is therefore underestimated. Furthermore, their strong radio continuum sources cause baseline ripple resulting in further uncertainty in the measured parameters.

The HI spectrum at the position of the nearby radio galaxy NGC 5128 represents the most difficult case. Due to the large extent and high flux density of its 20-cm radio continuum emission, the resulting (artificial) baseline ripple as well as the presence of HI absorption and extended HI emission over a large velocity range, the HI properties of NGC 5128 are difficult to measure. The fit to the HI position in HIPASS is very uncertain and offset by  $8'.9$  from the optical position (see Table 2). We used a 9th order baseline fit

to the original HI spectrum within a carefully selected velocity range to obtain the HI properties. The NGC 5128 HI spectrum shown by Gardner & Whiteoak (1976) was used to set the appropriate velocity range for the HI emission. The fitting results have large uncertainties. Using the same method as for the other BGC sources, we measure an integrated HI flux density of only  $91.8 \pm 13.2$  Jy km s<sup>-1</sup>, which is clearly an underestimate when compared with the HI measurements ( $F_{\text{HI}} = 122$  Jy km s<sup>-1</sup>) by van Gorkom et al. (1990). Schiminovich et al. (1994) in addition find HI emission associated with the diffuse shells of NGC 5128 and measure  $F_{\text{HI}} = 208$  Jy km s<sup>-1</sup>. The extended emission is also visible in the HIPASS data. Using a Gaussian fit we find an HI diameter of  $47'.5 (\pm 7'.3) \times 26'.1 (\pm 4'.0)$  at  $PA = 29^\circ$  and  $F_{\text{HI}} \approx 186$  Jy km s<sup>-1</sup> ( $M_{\text{HI}} = 9 \times 10^8 M_\odot$ ). The Local Group velocity of NGC 5128 is 338 km s<sup>-1</sup>, resulting in a distance of 4.5 Mpc. Recent estimates imply a closer distance of 3.5 Mpc (Hui et al. 1993).

We note that some galaxies with bright radio nuclei may be easily detected in HI absorption, but not in HI emission. Such galaxies would be missing from any HI peak-flux limited catalogs, despite their substantial HI content. An example is the edge-on disk galaxy NGC 5793 (HIPASS J1459–16A) which is not part of the BGC. It has an extremely luminous radio nucleus and is observed in HI absorption at velocities from 3420 to 3590 km s<sup>-1</sup> (see also Pihlstrom et al. 2000). A very weak emission feature at 3200 km s<sup>-1</sup> matches the blue-shifted H<sub>2</sub>O maser emission of NGC 5793 measured by Hagiwara et al. (1997). HI emission is also detected at  $\sim 2900$  km s<sup>-1</sup> (HIPASS J1459–16B) and is either associated with the elliptical galaxy NGC 5796 or an uncataloged neighbour to the East of NGC 5973.

### 3.7. Completeness and Reliability

The selection of sources for the BGC is based on their HI peak flux density ( $S_{\text{peak}} \gtrsim 116$  mJy). Since HIPASS has a uniform noise level of typically 13 mJy, BGC HI spectra generally have high signal-to-noise ratios (see Fig. 1). Identification and parameterization are both therefore expected to be highly reliable. Similarly, completeness is expected to be very high (see also Zwaan et al. 2003) with the exception of some areas of increased noise. These can arise from: residual narrow-band

interference; strong Galactic hydrogen recombination lines (see Section 3.7.1); scanning sidelobes north and south of bright extended HI sources (see Barnes et al. 2001); and residual baseline ripple at the position of strong radio continuum sources. As it affects all velocities, the latter is probably the most important, with the areas most affected being: (1) the Galactic Plane ( $|b| < 1^\circ$ ), particularly the spiral arm regions where the 20-cm radio continuum emission is very high; (2) the locations of individual strong radio continuum sources, some of which are the nuclei of gas-rich galaxies (e.g., NGC 5128, see Section 3.6). Within the BGC velocity range, only  $\sim 2.5\%$  of all southern HIPASS spectra have an r.m.s. noise greater than 23 mJy, i.e. at this noise level HI sources in the BGC are still detected with  $S_{\text{peak}} > 5\sigma$ . This gives a useful upper limit to the incompleteness of the BGC. For comparison, Fig. 2 shows a histogram of the clipped r.m.s. as measured in the spatially and spectrally integrated HI spectra of all BGC sources.

The HI peak flux density distribution (Fig. 8) is well described by an Euclidean power law ( $N \propto S_{\text{peak}}^{-2.5}$ ) suggesting that the BGC is complete. The best-fit linear regression to the log-log version of the histogram gives a slope of  $-2.57 \pm 0.12$  and an offset of  $0.040 \pm 0.073$ . The fit results vary with bin size and the number of bins, but are well reflected by the given error bars as long as each bin has a sufficient number of sources. Note that  $S_{\text{peak}}$  varies with velocity resolution and is affected by the noise of the HI spectrum.

The velocity-integrated HI flux density of a galaxy,  $F_{\text{HI}}$ , is a much more useful physical measurement than  $S_{\text{peak}}$ , because it relates more directly to its HI mass:  $M_{\text{HI}} \propto F_{\text{HI}} D^2$ . The  $F_{\text{HI}}$  distribution (Fig. 9) can be described by the same power law ( $N \propto F_{\text{HI}}^{-2.5}$ ) as the  $S_{\text{peak}}$  distribution but only for HI sources with  $F_{\text{HI}} \gtrsim 25$  Jy km s<sup>-1</sup>. This limit gives a highly complete subsample of  $\sim 500$  BGC sources. Whereas the BGC completeness limit is quite well defined the slope of the distribution is rather uncertain (and not well reflected in the given error bar). The best-fit linear regression to the log-log version of the histogram gives a slope of  $-2.47 \pm 0.13$  and an offset of  $5.54 \pm 0.23$ . We note that HICAT contains twenty HI sources with  $F_{\text{HI}} > 25.0$  Jy km s<sup>-1</sup> that are not listed in the BGC. These have  $S_{\text{peak}} < 116$  mJy

(the BGC  $S_{\text{peak}}$  cutoff) and 20% velocity widths greater than  $\sim 400 \text{ km s}^{-1}$ . This suggests that the  $F_{\text{HI}}$ -limited BGC sub-sample is about 95% complete.

In any H I peak flux limited sample, like the BGC, sources at a given integrated H I flux density are detected more easily the narrower their velocity widths are (see Fig. 10). This favours the detection of sources that are either intrinsically narrow-lined or galaxies viewed close to face-on. On the other hand, sources with a velocity width smaller than the HIPASS velocity resolution of  $18 \text{ km s}^{-1}$  and low signal to noise are very difficult to detect because the spectrum is likely to resemble noise or interference. The peak flux selection therefore means that the lowest integrated H I flux densities are found in galaxies with rather narrow profiles (typically  $w_{50} < 40 \text{ km s}^{-1}$ ), as shown in Fig. 10. From the work by Ryan-Weber et al. (2002) we know that many of the narrow-lined sources in the BGC are late-type dwarf galaxies, either previously uncatalogued or without prior velocity information. For example, we determined new velocities for 8 out of the 10 galaxies with the lowest  $F_{\text{HI}}$  values; these galaxies are generally under-represented in optical surveys because of their small diameters and low surface-brightness. The optical properties for all BGC sources, such as morphological types, inclination angles, and luminosities, will be presented in a later paper.

### 3.7.1. Velocity coverage

Because of confusion with Galactic gas, the BGC includes galaxies with  $|v_{\text{sys}}| < 350 \text{ km s}^{-1}$  only where these objects were previously known (and meet the BGC selection criteria). As such, the BGC may not be complete in this velocity range.

Putman et al. (2002) cataloged H I objects with  $|v_{\text{LSR}}| < 500 \text{ km s}^{-1}$  (mostly HVCs), excluding only  $|v_{\text{LSR}}| < 90 \text{ km s}^{-1}$ , and identified 40 galaxies. Among them are two newly cataloged galaxies: HIPASS J0746–28 (HIZSS 021, Henning et al. 2000) and HIPASS J1337–39 in the Centaurus A Group (see also Banks et al. 1999). Objects were classified as galaxies based on either being cataloged in LEDA or NED or being visible in the Digitized Sky Survey (DSS). Since this classification was based on optical data, some previously uncataloged galaxies (especially in the ZOA) may

have been mis-classified as HVCs. The BGC contains 37 H I objects with  $v_{\text{sys}} < 500 \text{ km s}^{-1}$ , six of which are newly cataloged objects including three H I clouds (see Table 4). That means there may be undiscovered low-velocity or Local Group galaxies missing from the BGC with  $|v_{\text{sys}}| < 350 \text{ km s}^{-1}$ .

We did not search for objects with  $v > 8000 \text{ km s}^{-1}$ . This limit, rather than the  $12700 \text{ km s}^{-1}$  limit of HIPASS, was set for practical reasons: the residual continuum ripple is worse at high velocities and occasional emissions from the GPS L3 beacon at velocities of  $\sim 8200 \text{ km s}^{-1}$  cause many false detections in MULTIFIND. Whilst visual inspection of the data cubes easily eliminates such candidates, the extra work of searching this, and higher velocities, was not considered worthwhile given the extremely low probability of detection (a face-on galaxy with a velocity width of  $50 \text{ km s}^{-1}$  would need to have an H I mass more than  $2 \times 10^{10} M_{\odot}$  to be included in the BGC). The HIPASS Catalog (Meyer et al. 2004) contains  $\sim 100$  galaxies with H I systemic velocities larger than  $8000 \text{ km s}^{-1}$ , all of which lie below the BGC peak flux cutoff.

The Galactic hydrogen recombination lines H166 $\alpha$ , H210 $\beta$  and H167 $\alpha$  occur within the BGC velocity range at frequencies which, if interpreted as a velocity, correspond to  $-911$ ,  $4340$ ,  $4507 \text{ km s}^{-1}$  (for an example see Fig. 11). Recombination lines are narrow, and generally restricted to regions of strong thermal emission in the Galactic Plane. So narrow velocity-width galaxies behind the Galactic Plane can be difficult to identify at some velocities. However, because of their distinctive spectrum, H II regions and other regions with recombination line emission are easily removed from the BGC.

## 4. Results & Discussions

In the following we briefly discuss the newly cataloged galaxies and H I clouds (Section 4.1) as well as the galaxies with the largest angular sizes (Section 4.2). Section 4.3 is devoted to the H I properties of the BGC sources. In Section 4.4 we compare the integrated H I flux density measurements in the HIPASS BGC to those in the literature, where available.

#### 4.1. Newly Cataloged Galaxies & HI Clouds

For 91 BGC members NED has no catalog entry; 87 of these are most likely galaxies (see below). The remaining four new sources appear to be HI clouds without optical counterparts. Three of these lie outside the Zone of Avoidance: HIPASS J1712–64 (Kilborn et al. 2000), J1718–59 (Koribalski 2001) and J0731–69 (Ryder et al. 2001); the fourth one is J1616–55 (Staveley-Smith et al. 1998). Their HI parameters are listed in Table 4.

Whereas HIPASS J0731–69 has been identified as a potential tidal cloud near NGC 2442, the others are at much lower velocities ( $v_{\text{sys}} < 500 \text{ km s}^{-1}$ ). HIPASS J1718–59 ( $\sim 3^\circ$  in length) lies only a few degrees away from J1712–64, but at a slightly lower systemic velocity. Together with J1616–55 and other, much weaker clouds at similar velocities, these objects could be tidal debris related to the Magellanic Clouds and the Leading Arm (Putman et al. 1998). The failure of deep observations by Lewis et al. (2002) to detect any stars in J1712–64 tends to confirm this theory.

Of the 87 likely new galaxies, 57 ( $\sim 70\%$ ) lie at Galactic latitudes below  $10^\circ$ . These constitute a substantial fraction of the total of 154 BGC members in this region. Fig. 12 shows a histogram of the galaxy latitudes. There are 37 BGC objects with  $|b| < 5^\circ$ , of which 32 are Henning et al. (2000) HIZSS galaxies (counted as ‘new’ for the purposes of this paper). The five additional galaxies are HIPASS J1526–51 ( $v_{\text{sys}} = 605 \text{ km s}^{-1}$ ; also known as HIZOA J1526–51, see Juraszek et al. 2000), J1441–62 ( $672 \text{ km s}^{-1}$ ), J1758–31 ( $3316 \text{ km s}^{-1}$ ), J1812–21 ( $1533 \text{ km s}^{-1}$ ), and J1851–09 ( $5485 \text{ km s}^{-1}$ ); no optical counterparts have as yet been identified for these. They were most likely missed in the HIZSS because of their very narrow HI profiles ( $w_{50} \approx 40\text{--}50 \text{ km s}^{-1}$ ; except HIPASS J1851–09 for which we measure  $w_{50} = 90 \text{ km s}^{-1}$ ).

Although most of the newly cataloged galaxies lie in or close to the Zone of Avoidance, some are near individual bright stars. Narrow HI velocity widths are typical for most of the newly cataloged galaxies outside the ZOA. This, together with their morphology suggests they are mostly dwarf irregular galaxies. Of the 21 new galaxies with  $|b| > 15^\circ$ , only one (HIPASS J0546–68) has

no obvious optical counterpart as it lies behind the Large Magellanic Cloud. For a detailed analysis of all the newly cataloged galaxies see Ryan-Weber et al. (2002).

#### 4.2. Extended BGC Sources

We find at least 24 BGC sources to be extended when compared to the Parkes beam of  $15.5'$ ; these are listed in Table 5. Although they have the largest angular sizes, mostly due to their proximity, only a few of them are physically large. BGC sources with very large angular sizes, like the Circinus galaxy (HIPASS J1413–65), may have their HI flux density underestimated due to strong negative sidelobes, an artifact of the bandpass calibration (see Barnes et al. 2001). In Table 5 we give their deconvolved Gaussian HI diameters as well as some of their HI properties, which are also listed in Table 2. The diameters were determined from a Gaussian fit to the integrated HI intensity distribution and represent, in nearly all cases, a good fit to the HIPASS data. For most HIPASS sources in Table 5 we give the fitted HI major and minor axes diameters as well as the position angles,  $PA$ . For sources which are resolved in one direction only, we list the fitted HI major axis diameter. Most of the extended sources in the BGC are nearby, well studied spiral galaxies, the largest of which is NGC 6744 (HIPASS J1909–63a). In addition, there are (at least) four extended galaxy pairs/groups and two HI clouds. Note that the extended HI envelope of a galaxy can greatly exceed the fitted Gaussian HI diameter. All extended sources are briefly described in Appendix B.1.

#### 4.3. HI Properties

##### 4.3.1. Peak and Integrated HI Flux Densities

The ten HI-brightest galaxies in the BGC are, in order of their HI peak flux densities ( $S_{\text{peak}}$ ), NGC 6822, NGC 300, NGC 55, NGC 3109, Circinus, NGC 5236 (M83), the Wolf-Lundmark Melotte (WLM), NGC 3621, NGC 6744, and NGC 247. The list of galaxies with the highest integrated HI flux densities ( $F_{\text{HI}}$ ) is nearly identical (instead of the WLM it includes NGC 253). All are well-known, nearby spiral galaxies which, except for the WLM, are extended with respect to the Parkes beam (see Tables 3 & 5). For comparison, the optically brightest

galaxies (according to their blue magnitude as listed in LEDA), are NGC 5128, NGC 5236, NGC 253, NGC 300, NGC 4594, ESO356-G004 (Fornax dwarf spheroidal), NGC 6744, NGC 4945, NGC 6822, and NGC 1068. While there are several sources in common, three of the optically brightest galaxies (NGC 4594, ESO356-G004, and NGC 1068) did not make it into the BGC, emphasizing again that there are many optically bright (elliptical) galaxies with little H I gas. Histograms of the H I peak and integrated flux densities of the BGC sources are shown in Figs. 8 and 9, respectively, and are discussed in Section 3.7.

#### 4.3.2. HI Velocity Distribution

Fig. 13 shows the BGC H I Local Group velocity histogram for all 1000 sources as well as for the complete  $F_{\text{HI}}$ -limited sub-sample ( $F_{\text{HI}} > 25 \text{ Jy km s}^{-1}$ , see Section 3.7). We overlaid the selection functions as derived by Zwaan et al. (2003, see their Fig. 17) based on the BGC H I mass function. Several overdensities are clearly visible indicating significant structure in the nearby galaxy distribution (see Section 5).

For comparison we show in Fig. 14 the H I systemic velocity histograms from the targeted samples of Mathewson et al. (1992) and Theureau et al. (1998). While some local structure is clearly visible, it differs significantly from that seen in the BGC due to selection effects. Note that MFB92 target Sb–d galaxies with inclination angles  $i > 40^\circ$  and Galactic latitudes  $|b| > 11^\circ$ , selected mainly from optical catalogs, while Theureau et al. (1998) target more distant Sa–Sdm galaxies. The differences between the BGC velocity histogram and that of the optical comparison sample obtained from LEDA are discussed in Section 5.

Galaxies with low systemic velocities are of particular interest as they are very close and can be studied in detail (see also Section 5). The BGC contains about 50 (160) galaxies within a distance of 5 (10) Mpc many of which are located in the Local Group, the Sculptor Group or the Centaurus A Group. There are many other nearby groups, e.g. the NGC 3056 group ( $10^{\text{h}}, -30^\circ$ ,  $v_{\text{sys}} \sim 950 \text{ km s}^{-1}$ , overlapping with LGG 180) with around ten H I-rich members, but none as prominent as the Sculptor or Centaurus A Groups.

In addition to the Magellanic Clouds, we de-

tected four *Local Group* galaxies in the HIPASS BGC (see Table 3) out of the 36 listed by van den Bergh (2000): these are the dwarf irregular galaxies NGC 6822 (DDO 209; see Section 4.2), DDO 210 (Aquarius Dwarf), WLM (DDO 221) and ESO594-G004 (SagDIG, see Young & Lo 1997). The remaining six southern Local Group members are gas-poor dwarf spheroidal galaxies. Further away, in the outskirts of the Local Group, we detected the dwarf irregular galaxies IC 5152, Sextans A and NGC 3109 (see Appendix B.1 and B.2). No optical identification has so far been obtained for the galaxy HIZSS 003 ( $b = 0^\circ 1$ ) which lies at a distance of  $\sim 1.5$  Mpc.

Of the 35 potential *Sculptor Group* members in the velocity range from zero to  $800 \text{ km s}^{-1}$  we detected 25 (20 of which are part of the BGC), six were not detected and four objects (SC 02, SC 18, SC 24, and SC 42) were discarded because the neutral hydrogen gas at the published velocities (Coté et al. 1997) appears to be part of an HVC complex.

Banks et al. (1999) searched for galaxies in the *Centaurus A Group* using HIPASS data. They detected H I in 30 galaxies, nine of which were identified as new group members. Four galaxies were previously uncataloged: HIPASS J1321–31, J1337–39, J1348–37 and J1351–47; the first two are also in the BGC. In total, the BGC contains at least 21 Centaurus A Group members (incl. NGC 5128, see Section 3.6).

#### 4.3.3. HI Mass Distribution

Fig. 15 shows the BGC H I mass distribution for all 1000 sources as well as for the complete  $F_{\text{HI}}$ -limited sub-sample. The derived H I masses range from  $2 \times 10^6 M_\odot$  to  $4 \times 10^{10} M_\odot$ . The BGC sources with the highest H I masses are described in Appendix B.3. We find a median  $M_{\text{HI}}$  of  $2.9 \times 10^9 M_\odot$  ( $\log M_{\text{HI}} = 9.46$ ), similar to the H I mass of the Milky Way, for all BGC sources, and a slightly higher value of  $3.9 \times 10^9 M_\odot$  ( $\log M_{\text{HI}} = 9.59$ ) for the complete sub-sample. The BGC H I mass function (Zwaan et al. 2003) is characterized by a Schechter function with a slope of  $\alpha = -1.30 \pm 0.08$  and a "knee" of  $\log (M_{\text{HI}}^* / M_\odot) = 9.79 \pm 0.06$ .

Figs. 16 and 17 show the  $M_{\text{HI}}$  distribution of all BGC sources with respect to their distance,  $D$ , and velocity width,  $w_{50}$ . In Fig. 16, which illus-

trates the depth of our HI sample, we have indicated the approximate detection limit of the BGC ( $F_{\text{HI}} \approx 5 \text{ Jy km s}^{-1}$ ) as well as the  $F_{\text{HI}}$  completeness limit ( $F_{\text{HI}} = 25 \text{ Jy km s}^{-1}$ ). Note that the HI peak flux density cutoff,  $S_{\text{peak}} = 116 \text{ mJy}$ , of the BGC is similar to the  $5\sigma$  detection limit of the HI survey by Fisher & Tully (1981a). Fig. 16 is closely matched to figure 1 of Briggs (1997) who compared the depths of several HI-rich galaxy samples. Fig. 17 shows the selection effects due to the peak flux limited nature of our sample as well as a strong correlation between the HI velocity width and the HI mass of galaxies. Note that we display the measured velocity widths uncorrected for galaxy inclination. At a given HI flux density (HI mass), the BGC is biased towards sources with low velocity width, and, vice versa, at a given velocity width it is biased towards galaxies with high  $F_{\text{HI}}$  ( $M_{\text{HI}}$ ); see also Fig. 10.

Only 3 (38) sources in the BGC have HI masses below  $10^7$  ( $10^8$ )  $M_{\odot}$ , of these 1 (10) were previously uncatalogued. The galaxies with the lowest HI masses are DDO 210 (Aquarius dwarf), HIPASS J1247-77 (see Kilborn et al. 2002), ESO594-G004 (SagDIG), ESO349-G031 (SDIG), NGC 5237, HIZSS 003, IC 3104, UGCA 015 (DDO 006), ESO383-G087 and HIPASS J1337-39 (Banks et al. 1999). They are typically nearby late-type dwarf galaxies, characterized by very narrow HI velocity widths and  $v_{\text{sys}} < 500 \text{ km s}^{-1}$ .

#### 4.3.4. HI Velocity Width Distribution

Fig. 18 shows a histograms of the 50% and 20% HI velocity widths,  $w_{50}$  and  $w_{20}$ , respectively. While  $w_{50}$  is usually a very robust measurement for the BGC sources,  $w_{20}$  is more easily affected by noise and/or confusion by companions within the Parkes beam. We find a mean width of  $\langle w_{50} \rangle = 173 \text{ km s}^{-1}$  ( $\sigma = 106 \text{ km s}^{-1}$ ) and  $\langle w_{20} \rangle = 210 \text{ km s}^{-1}$  ( $\sigma = 116 \text{ km s}^{-1}$ ). The median values for  $w_{50}$  and  $w_{20}$  are  $\sim 20 \text{ km s}^{-1}$  lower:  $155 \text{ km s}^{-1}$  and  $191 \text{ km s}^{-1}$ , respectively. The BGC sources with the largest measured 50% and 20% velocity widths are described in Appendix B.4. For comparison we also show the distribution of the measured velocity widths in the complete  $F_{\text{HI}}$ -limited sub-sample of the BGC. Their mean values are  $\langle w_{50} \rangle_{\text{sub}} = 228 \text{ km s}^{-1}$  ( $\sigma = 108 \text{ km s}^{-1}$ ) and  $\langle w_{20} \rangle_{\text{sub}} = 269 \text{ km s}^{-1}$  ( $\sigma = 119 \text{ km s}^{-1}$ ), significantly higher than for all BGC sources. The me-

dian values are  $212 \text{ km s}^{-1}$  ( $w_{50}$ ) and  $253 \text{ km s}^{-1}$  ( $w_{20}$ ). Henning (1995) obtained mean 50% line widths for five different galaxy samples, ranging from  $\langle w_{50} \rangle_{\text{LSB}} = 155 \text{ km s}^{-1}$  ( $\sigma = 82 \text{ km s}^{-1}$ ) for the LSB sample to  $\langle w_{50} \rangle_{\text{IRAS}} = 288 \text{ km s}^{-1}$  ( $\sigma = 124 \text{ km s}^{-1}$ ) for the IRAS sample, clearly showing the effects of source selection. While the  $F_{\text{HI}}$ -limited sub-sample has an intermediate mean width, suggesting it is drawn from a population of large spirals and dwarf galaxies, the remaining sources in the BGC are mainly drawn from a population of late-type galaxies.

#### 4.3.5. The Shape of HI Profiles

The ratio of the 20% and 50% velocity widths (see Fig. 19) gives an indication of the HI profile shape, in particular the steepness of the profile edges. The steepest edges are typically found in regular spiral galaxies with extended, flat rotation curves, resulting in well-defined double horn profiles (e.g. HIPASS J0833-22 = NGC 2613,  $w_{20} / w_{50} = 1.03$ ), while irregular dwarf galaxies tend to show Gaussian profiles (e.g. HIPASS J0919-12 = DDO 060,  $w_{20} / w_{50} = 1.53$ ). The median  $w_{50} / w_{20}$  ratio in the BGC is 1.18. The HI profiles of galaxy pairs/groups and confused galaxies generally show much higher ratios. Values of  $w_{20} / w_{50} > 4$  were found in the irregular galaxy UGC 08127, and the groups HIPASS J2206-31 and J0605-14 (see Ryan-Weber et al. 2002). In these cases a narrow HI component is accompanied by a broad HI spectrum.

The HI spectrum of a single galaxy is determined by its HI distribution, velocity field and inclination. While a symmetric HI spectrum usually indicates a symmetric, regular rotating galaxy, an asymmetric HI spectrum can be due to a variety of internal and external factors (e.g., asymmetric HI distribution, irregular rotation pattern, warps, neighboring HI sources) which are best investigated using interferometric HI data (see, e.g., Baldwin et al. 1980, Swaters et al. 2002). Richter & Sancisi (1994) as well as Haynes et al. (1998) find that (at least) half of the single-dish HI spectra obtained for large samples of galaxies show significant asymmetries. Following Haynes et al. we use the fractional velocity difference criterion,  $|v_{\text{sys}} - v_{\text{mom1}}| / w_{50} > 0.02$ , to estimate the approximate number of asymmetric HI profiles in the BGC. Here  $v_{\text{sys}}$  is the HI systemic velocity,

measured at the midpoint of the 50% level of the peak flux density (see Table 2), and  $v_{\text{mom}1}$  is the first moment. We find the HI spectra of half the BGC sources to be asymmetric, in agreement with previous studies. For about a quarter of BGC HI spectra we calculate a fractional velocity difference larger than 0.04. Fig. 1 shows a large range of spectral shapes, ranging from symmetric over mildly asymmetric to severely distorted. We find that the difference criterion is not appropriate for BGC sources with narrow velocity widths. Nevertheless, after excluding HI sources with  $w_{50} > 90 \text{ km s}^{-1}$ , we again find about half the remaining HI sources to be asymmetric. There are 70 BGC sources with  $w_{20} / w_{50} > 1.8$ , among them many galaxy pairs and groups, all of which fulfill the above asymmetry criterion.

#### 4.4. Comparison of HI fluxes with other surveys

Here we compare the  $F_{\text{HI}}$  measurements in the HIPASS BGC with those obtained by Mathewson et al. (1992) and Theureau et al. (1998) as well as with the 21-cm magnitudes given in LEDA, which includes the first two HI samples.

The BGC and the targeted sample by MFB92 have 228 galaxies in common, although some galaxies are confused by neighbouring sources. Fig. 20 shows the percentage difference between  $F_{\text{HI,BGC}}$  and  $F_{\text{HI,MFB92}}$ . The median offset from zero is  $-9\%$ , consistent with the difference in absolute flux calibration (see Section 2.1).

Theureau et al. (1998), who observed over 1200 southern galaxies in HI with the Nançay telescope (HPBW =  $3'6 \times 22'$  at  $\delta = 0^\circ$ ), use numerous "calibrating galaxies", three of which are also in the BGC. For NGC 1518, NGC 1637, and NGC 6814 they measure  $F_{\text{HI,T98}} = 50.66, 38.43, \text{ and } 21.03 \text{ Jy km s}^{-1}$ , respectively, whereas we measure  $F_{\text{HI,BGC}} = 72.0 \pm 5.7, 72.4 \pm 5.9, \text{ and } 37.3 \pm 4.0 \text{ Jy km s}^{-1}$  (see Table 2),  $\sim 40\text{--}70\%$  larger than their values. Our  $F_{\text{HI}}$  measurements agree with those listed by Huchtmeier & Richter (1989). As the HI envelopes of galaxies are typically a factor two larger than their optical diameters (see, e.g., Salpeter & Hoffman 1996), it is likely that only a fraction of the galaxy HI extent was detected within the Nançay telescope beam.

We found LEDA 21-cm magnitudes,  $m_{21}$ , for

692 galaxies in the BGC, where  $m_{21} = 17.4 - 2.5 \log(F_{\text{HI}})$ . The mean of the  $m_{21}$  uncertainties quoted in LEDA is 0.22 ( $\sigma = 0.08$ ) or 22%  $F_{\text{HI}}$ . For galaxies with multiple  $F_{\text{HI}}$  measurements, a general LEDA search outputs a single, preferred value. The percentage difference between  $F_{\text{HI,BGC}}$  and  $F_{\text{HI,LEDA}}$  is shown in Fig. 21. The median of the distribution is  $+0.8\%$ , showing good agreement with other HI data for the majority of galaxies. For nearly 80% of the BGC sources the  $F_{\text{HI}}$  difference is less than 25%. If we ignore any sources which differ by more than 40% in  $F_{\text{HI}}$ , the mean difference of the remaining 610 sources is  $-0.06\%$  ( $\sigma = 15.2\%$ ).

The largest  $F_{\text{HI}}$  difference occurs for the edge-on spiral galaxy MCG-02-14-003 (HIPASS J0511-09) which has an HI flux density of  $30.1 \text{ Jy km s}^{-1}$  (BGC), in agreement with MFB92 who measure  $F_{\text{HI}} = 30.65 \text{ Jy km s}^{-1}$ . The value of  $F_{\text{HI}} = 2.4 \text{ Jy km s}^{-1}$  stated by Theureau et al. (1998) is likely to be a typographical error as their HI spectrum is similar to ours. Discrepancies were already noted for HIPASS J0622-07 (for which CGMW1-0080 is not the correct optical counterpart; see Section 3.5) and HIPASS J1324-42 (NGC 5128, for which the standard fitting routine severely underestimates the total HI flux density). We found the published HI flux densities for the galaxies with the largest discrepancies, ESO001-G006 (MFB92), ESO274-G016 and ESO375-G071 (Fisher & Tully 1981) severely underestimated. For the latter two galaxies our  $F_{\text{HI}}$  measurements agree roughly with those by Longmore et al. (1982). The  $F_{\text{HI}}$  value quoted by Theureau et al. (1998) for the galaxy UGC04358 (see the left-most point on Fig. 21), is also a typographical error.

## 5. Large-Scale Structure

Here, we analyze the large-scale structures revealed by the HIPASS Bright Galaxy Catalog (BGC) and compare to the 1000 *optically*-brightest galaxies in the southern sky.

### 5.1. The optical comparison sample

The optical galaxy sample was defined using the Lyon/Meudon Extragalactic Database (LEDA), selecting the brightest galaxies based on their apparent total blue magnitudes ( $B_T$ ). There are

1000 southern galaxies with  $B_T \lesssim 13^m26$ : 38 of these have no velocities recorded in LEDA, five have velocities beyond the BGC limit of  $8000 \text{ km s}^{-1}$ . The HIPASS BGC and the LEDA comparison sample have only  $\sim 400$  galaxies in common. For  $\sim 600$  galaxies in the optical sample, 21-cm fluxes are listed in LEDA, indicating (1) a large fraction of gas-poor galaxies (see Koribalski 2002) and/or (2) a lack of (cataloged) HI measurements, probably both. Either way, it is clear that the HI- and optically-selected samples differ significantly in their properties.

Note also that the low angular resolution of single dish HI galaxy samples compared to optically selected galaxy samples results in numerous unresolved galaxy pairs and groups for the HIPASS BGC, while the LEDA sample is mostly composed of individual galaxies.

## 5.2. Galaxy distribution on the sky

Fig. 22 shows the sky distribution of the 1000 HI-brightest galaxies (the HIPASS BGC) and Fig. 23 that of the optical comparison sample. The sky distributions of the two samples show a broad similarity, but strongly differ in some details.

The first concerns the Zone of Avoidance (ZOA): the HI galaxies in the BGC give us the first view of the local Universe in the southern hemisphere uninhibited by the foreground stars and dust from our own Galaxy. Numerous known large-scale structures can be fully traced across the sky, the most prominent being the Supergalactic Plane (see Section 5.3.1), the second one certainly the Centaurus Wall which connects via the Hydra and Antlia clusters to the Puppis filament crossing the ZOA in two locations (two of the dinosaur’s toes as pointed out by Lynden-Bell 1994). The structures also allow a much improved delineation of voids as for example in the case of the Local Void (see Section 5.3.4). Amazingly enough it is not only behind the Milky Way that new structures can be mapped for the first time. Some previously hardly noticed galaxy groups stand out quite distinctively in the HI sky distributions. These are discussed in further detail in the description of the various velocity slices (see Fig. 24).

The second striking point concerns the cluster-

ing properties of the two samples: although both follow overall the same structures, the HI distribution appears much more homogeneous and less clumpy than the optical one. This is due to the fact that (a) the optical sample contains many more elliptical and early-type galaxies than the HIPASS BGC which is dominated by late-type spiral galaxies (see Koribalski 2002), and (b) early-type galaxies mark the bottoms of the potential wells of the high density peaks in the Universe (from rich groups to clusters) whereas the spiral or irregular galaxies — although also found in clusters and rich groups — are the main building blocks of poor groups of galaxies and particularly the filamentary cellular-like structures that seem to connect groups and clusters. A study of the statistical properties of both samples is under way.

A more subtle reason for the discrepancy in the distribution lies in the respective velocity histograms (see Fig. 25). The peak of the velocity distribution of the BGC lies at a very low  $v_{\text{hel}} \sim 1600 \text{ km s}^{-1}$  (width  $\sim 600 \text{ km s}^{-1}$ ), preceded by a secondary maximum of  $v_{\text{hel}} \sim 900 \text{ km s}^{-1}$  (width  $\sim 300 \text{ km s}^{-1}$ ). This results in a sharp drop-off for  $v_{\text{hel}} \gtrsim 2000 \text{ km s}^{-1}$  and little sensitivity to structures beyond  $3000 \text{ km s}^{-1}$ . With less than 50 galaxies with  $v_{\text{hel}} > 4000 \text{ km s}^{-1}$ , the BGC has no power to make predictions about the Great Attractor (GA) region and its overdensity with respect to the remaining part of the southern sky. The mean velocity in the BGC is  $\sim 1900 \text{ km s}^{-1}$  ( $\sigma \sim 1000 \text{ km s}^{-1}$ ). The optical comparison sample has a considerably higher mean of  $\sim 2300 \text{ km s}^{-1}$  ( $\sigma \sim 1300 \text{ km s}^{-1}$ ), with peaks around  $1600 \text{ km s}^{-1}$  and  $2600 \text{ km s}^{-1}$ , and a slight excess, compared to the BGC, of sources around  $\sim 4200 \text{ km s}^{-1}$ . The center of the GA overdensity remains obscured because of the Milky Way.

An interesting, though not intuitive, result of this difference in the velocity distribution is the fact that the BGC samples the very nearby Universe much deeper than a similarly defined optical sample: the HI galaxy sample contains nearly 1.5 times more galaxies within  $v_{\text{hel}} < 2000 \text{ km s}^{-1}$  than its optical counterpart even though the latter contains early-type galaxies and gas-poor dwarfs as well. And while the overall appearance of the BGC is less clumpy, it actually outlines structures in the very *nearby* Universe with much greater

precision and homogeneity, and fewer gaps (see e.g. the Supergalactic Plane in the top panel of Fig. 24).

In the following the most prominent structures are described in a sequence of increasing velocity intervals.

### 5.3. The nearest velocity slice ( $v < 1400 \text{ km s}^{-1}$ )

The top panel of Fig. 24 shows the distribution of the galaxies with velocities below  $1400 \text{ km s}^{-1}$ . The most prominent features are the Supergalactic Plane (SGP), the Local Void next to the Puppis filament, the near side of the Fornax Wall and the Volans Void (see also Table 6).

#### 5.3.1. The Supergalactic Plane

The Supergalactic Plane (SGP) contains the greatest concentration of nearby groups and clusters of galaxies in the local Universe (see Lahav et al. 2000, and references therein). It is partly a projection of the Local Supercluster with the Virgo cluster near its center and the Local Group and the Sculptor Group at its outer boundary and partly a projection of the more distant Centaurus Wall. The SGP was defined by de Vaucouleurs in the 1950’s based on a study of the Shapley-Ames Catalog of the brightest 1246 galaxies in the whole sky. He noted its flattened pancake-like structure and defined a coordinate system centered on this structure. The Supergalactic equator (see de Vaucouleurs et al. 1991 for its definition) is shown as the horizontal line in Figs. 22, 23 and 24. We can clearly see that the nearest galaxies (top panel) follow this line closely. Interestingly enough it has been found in the last two decades that the concentration of galaxies towards the SGP continues out to larger distances and that the two dominant structures, the GA and Perseus-Pisces superclusters, also lie along this equator.

The SGP is very evident in galaxies from the BGC which form a distinct and continuous filamentary band — without a gap due to the ZOA — across the whole southern sky ending on the righthand side in the Southern Virgo Extension ( $\alpha, \delta(\text{J2000}) = 12^{\text{h}}5, -5^{\circ}$ ,  $v_{\text{hel}} \sim 1100 \text{ km s}^{-1}$ ) which is quite a dominant agglomeration in this slice. Beside this clumping, the width of the band is no more than  $\sim 10^{\circ}$ . Deviations of up to  $10^{\circ} - 15^{\circ}$  from the supergalactic equator are apparent.

#### 5.3.2. The Puppis filament

There is a suggestion in this sky projection that the SGP might be 2-pronged with a second filament which folds back across the ZOA in Puppis ( $8^{\text{h}}, -30^{\circ}$ ), seemingly encircling the Fornax Wall described below. The latter circle, which contains the here fully revealed Puppis filament, rises in significance due to two previously unrecognized galaxy groups in Antlia (centered at  $\sim 900 \text{ km s}^{-1}$  and  $\alpha, \delta(\text{J2000}) = 9^{\text{h}}50^{\text{m}}, -30^{\circ}$  and  $10^{\text{h}}40^{\text{m}}, -37^{\circ}$ , respectively) which we suggest to be named the Antlia G1 and Antlia G2 groups. They contain spiral galaxies with HI masses of the order of  $10^8 M_{\odot}$  and are hardly visible in optical surveys. Antlia G1 might be related to the Antlia Cloud although the grouping visible in the BGC does not coincide with the members listed in Tully (1982). The extension of the Puppis filament through these two groups seems to connect with the SGP at about  $13^{\text{h}}30^{\text{m}}, -30^{\circ}$ . It is conceivable that the Puppis filament also connects to the slightly higher velocity Southern Virgo Extension.

#### 5.3.3. The Fornax Wall

Another important feature in the nearby Universe is the Fornax Wall. It consists of the nearby Dorado Cloud and is quite extensive on the sky. It is made of three loose galaxy groups centered on NGC 1672 ( $\alpha, \delta(\text{J2000}) = 4^{\text{h}}45^{\text{m}}, -59^{\circ}$ ), NGC 1566 ( $4^{\text{h}}20^{\text{m}}, -55^{\circ}$ ) and NGC 1433 ( $3^{\text{h}}40^{\text{m}}, -47^{\circ}$ ) and extending in velocity space from 900 to about  $1200 \text{ km s}^{-1}$ , to the compact Fornax cluster ( $3^{\text{h}}40^{\text{m}}, -36^{\circ}$ ,  $\sim 1300 \text{ km s}^{-1}$ ) towards the slightly higher-velocity Eridanus Cloud ( $\sim 1800 \text{ km s}^{-1}$ ) centered on NGC 1332 ( $3^{\text{h}}24^{\text{m}}, -22^{\circ}$ ). Fornax and Eridanus are still visible in the middle panel.

#### 5.3.4. The Local Void

The HIPASS Bright Galaxy Catalog also is much more stringent in defining the void sizes. The dominant void in the nearby Universe clearly is the Local Void which can be seen as the empty region above the SGP in the top and middle panels of Fig. 24.

The existence of the “Local Void” was first pointed out by Tully & Fisher (1987). They studied the sky distribution of galaxies within  $cz = 3000 \text{ km s}^{-1}$  and discovered that relatively few galaxies lie in the region between  $l = 0 - 90^{\circ}$ ,  $b$

$= -30^\circ$  to  $+30^\circ$ . Because the great portion of the Local Void is located behind the Milky Way, its size and distance have not been definitely measured. The Local Void might be relevant to the origin of the “Local Anomaly” motion (see, e.g., Faber & Burstein 1988). Nakanishi et al. (1997) find the center of the Local Void to be located at  $l, b = 60^\circ, -15^\circ$ , and  $v_{\text{hel}} = 2500 \text{ km s}^{-1}$ , and the size is  $\sim 2500 \text{ km s}^{-1}$  along the direction toward the center. Whereas Fairall (1998) gives the center of the Local Void to be located at  $l, b = 18^\circ, 6^\circ$  ( $\alpha, \delta(\text{J2000}) = 18^{\text{h}}, -10^\circ$ ), and  $v_{\text{hel}} = 1500 \text{ km s}^{-1}$ , emphasizing herewith the difficulty in assessing its true dimensions.

The BGC enables us to redefine the extent of the Local Void as approximately  $l \sim -10^\circ$  to  $+20^\circ$ ,  $b \sim -20^\circ$  to  $+20^\circ$  and  $v_{\text{hel}} \lesssim 1700 \text{ km s}^{-1}$  (see Fig. 26). For  $b \sim -20^\circ$  to  $0^\circ$  the void appears to extend up to  $l = 30^\circ - 40^\circ$ . Fig. 24 reveals its size to be clearly smaller in the HI sky compared to the optical, mainly because the latter is strongly affected by Galactic extinction. The HIPASS BGC reveals the outer boundary of the Local Void (opposite the SGP in Fig. 24) which is hidden in optical surveys due to the broad ZOA in that region ( $\pm 25^\circ$ ) caused by the Galactic Bulge (see Fig. 1 in Kraan-Korteweg & Lahav 2000). We find nine previously uncataloged galaxies in the range  $l = 0$  to  $+40^\circ$  and  $|b| < 20^\circ$ , six of which lie at velocities of  $1500 - 1700 \text{ km s}^{-1}$ .

### 5.3.5. The Volans Void

Similarly to the Local Void, the Volans Void (see “Atlas Section” in Fairall 1998) centered at  $\alpha, \delta(\text{J2000}) = 7^{\text{h}} 00^{\text{m}}, -70^\circ$ ,  $\sim 800 \text{ km s}^{-1}$  is quite extensive in the optical (seen most clearly in the top right panel, below the SGP) but seems to be cut in half with galaxies identified in the BGC (top left panel).

### 5.4. The middle velocity slice ( $2200 > v > 1400 \text{ km s}^{-1}$ )

The middle panel of Fig. 24 shows galaxies with velocities between  $1400$  and  $2200 \text{ km s}^{-1}$ . In this range the BGC still probes deeper than the optical sample and reveals clear filamentary features while the optical galaxy distribution already loses the SGP as well as the Puppis filament. Besides the clumpings of Fornax, Eridanus and the Southern

Virgo Extension visible in both catalogs, the BGC finds two further galaxy groups which are not at all visible in the optical. They are found close to the Southern Virgo Extension at  $\alpha, \delta(\text{J2000}) = 12^{\text{h}} 00^{\text{m}}, -20^\circ$  and  $13^{\text{h}} 15^{\text{m}}, -20^\circ$ , respectively, both at a mean velocity of  $\sim 1750 \text{ km s}^{-1}$  with quite narrow velocity dispersions.

The first of the two groups has previously been identified as the NGC 4038 Group in the Crater Cloud (Tully 1988, Tully & Fisher 1987). Its brightest elliptical member (not detected in HIPASS) is NGC 3957 with  $B_{\text{T}} = 13^{\text{m}} 03$  at a velocity of  $1687 \text{ km s}^{-1}$ . It has over a dozen members in the BGC with HI masses ranging between  $1 - 10 \times 10^9 M_{\odot}$ .

The second galaxy group has not before been recognized as such, probably because it does lie exactly on the SGP. Being hardly prominent in the optical it must have been viewed as an element of the SGP rather than a galaxy group. This group contains close to a dozen spirals detected in the BGC with similar HI masses as for the NGC 4038 Group. Its brightest elliptical is the gas-rich galaxy NGC 5084 (HIPASS J1320–21),  $B_{\text{T}} = 11^{\text{m}} 55$ , at a velocity of  $1864 \text{ km s}^{-1}$  and we suggest that this new group be named after this galaxy, i.e. the NGC 5084 Group (see Table 6).

### 5.5. The highest velocity slice ( $v > 2200 \text{ km s}^{-1}$ )

In the bottom panel, which shows galaxies with velocities above  $2200 \text{ km s}^{-1}$ , the optical sample is more strongly populated than the BGC. Even so, the BGC seems to trace the structures in a smoother manner than the optical sample. This is primarily due to the fact that the main filament described below in further detail crosses the ZOA twice and hence is lost in optical surveys. Secondly, the filamentary structure in the optical sample is identified through a sequence of clumps, respectively of galaxy clusters, with few galaxies in between.

Again we have one dominant filament in this velocity slice which can be followed over a major fraction of the southern sky. It can be traced from the Indus and Pavo clusters ( $\alpha, \delta(\text{J2000}) = 21^{\text{h}} 00^{\text{m}}, -47^\circ$  and  $18^{\text{h}} 50^{\text{m}}, -63^\circ$ , respectively) crossing the ZOA to the Centaurus cluster ( $12^{\text{h}} 50^{\text{m}}, -40^\circ$ ) in a linear structure, called the Centaurus Wall by Fairall (1998), at a slight angle

with respect to the SGP. From there it bends over to the Hydra ( $10^{\text{h}} 40^{\text{m}}, -25^{\circ}$ ) and Antlia ( $10^{\text{h}} 30^{\text{m}}, -35^{\circ}$ ) clusters and folds back across the ZOA through Puppis where yet another spiral-rich new galaxy group is uncovered.

This galaxy group at  $7^{\text{h}} 50^{\text{m}}, -35^{\circ}$ , named here Puppis G2 lies at  $\sim 2800 \text{ km s}^{-1}$  and contains only newly identified galaxies (HIZSS plus new BGC galaxies). However, this agglomeration might point to a fairly massive group because at this velocity distance only the most HI-massive galaxies are revealed in the BGC (they indeed have HI masses between  $3 - 10 \times 10^9 M_{\odot}$ ) and with an optical extinction  $A_B$  of over 4 mag at this location, even the deep optical ZOA surveys are unlikely to uncover many of the possible early-type members of this group. This whole filament seems to encircle the Eridanus Void, a large void that extends out to about  $5000 \text{ km s}^{-1}$  (Fairall 1998).

It should be stressed again that the optical galaxy comparison sample probes the nearby Universe to much higher velocities which results in the fact that we may recognize high velocity features in the optical velocity slice to which the BGC is not sensitive anymore. This is quite notable for the Great Attractor region (centered on  $\alpha, \delta(\text{J2000}) = 15^{\text{h}} 00^{\text{m}}, -60^{\circ}, 4500 \text{ km s}^{-1}$ ) where the optical sample does show a preponderance of galaxies in the general direction of the Great Attractor overdensity — with a huge gap of its central part though, due to the ZOA. As stated above, the Great Attractor is not being traced by the BGC.

## 6. Conclusions

The HIPASS Bright Galaxy Catalog is a subset of HIPASS and contains the 1000 HI-brightest sources in the southern sky ( $\delta < 0^{\circ}$ ) based on their peak flux density ( $S_{\text{peak}} \gtrsim 116 \text{ mJy}$ ) as measured from the spatially integrated HI spectrum. We obtained previously catalogued optical (or infrared) counterparts for 909 of the 1000 BGC sources. The HIPASS BGC is the second largest sample of galaxies from a blind HI survey to date, covering a volume of  $\sim 2 \times 10^6 \text{ Mpc}^3$ , only surpassed by the HIPASS Catalog itself. While the BGC is complete in peak flux density, only a subset of  $\sim 500$  BGC members can be considered complete in integrated HI flux density ( $F_{\text{HI}} \gtrsim 25 \text{ Jy km s}^{-1}$ ).

The lowest detectable HI flux density for relatively narrow line-width sources in the BGC (galaxies as well as HI clouds) is given by  $F_{\text{HI}} = 0.7 \times S_{\text{peak}} \times w_{50}$  (see Fig. 10) corresponding to an HI mass of  $2 \times 10^4 w_{50} D^2$  (see Fig. 16). This means HI sources with  $w_{50} = 50 \text{ km s}^{-1}$  and  $M_{\text{HI}} \gtrsim 10^8 (10^9) M_{\odot}$  can be detected out to 10 (30) Mpc.

Of the 91 newly catalogued BGC sources, 87 appear to be galaxies. A large fraction of these (37) lie at Galactic latitudes  $|b| < 5^{\circ}$ ; all but five were previously uncovered by the HI Zone of Avoidance shallow survey (HIZSS; Henning et al. 2000). For all but one of the 30 *new* galaxies at  $|b| > 10^{\circ}$  optical counterparts were discovered in the Digitized Sky Surveys (see Ryan-Weber et al. 2002). For a further 51 galaxies in the BGC no redshifts were previously known. In addition, we identify 16 galaxies (i.e.,  $\sim 2\%$  of the BGC) where the catalogued optical velocity is potentially incorrect, resulting in a total of 158 new redshifts.

There are four HI clouds in the BGC, three of which are most likely Magellanic debris (HIPASS J1712–64, J1718–59, and J1616–55) with systemic velocities in the range  $390\text{--}460 \text{ km s}^{-1}$ . Further, detailed investigations are under way. We discovered one intergalactic HI cloud, HIPASS J0731–69, which is associated with the galaxy NGC 2442 (Ryder et al. 2001). The cloud, which lies at a projected distance of  $38'$  (176 kpc) from NGC 2442 ( $D = 15.9 \text{ Mpc}$ ) has an HI mass of nearly  $10^9 M_{\odot}$ . We could have detected similar HI clouds up to a distance of 30 Mpc, with a separation of at least  $20'$  from an associated HI-rich galaxy. This detection suggests that their space density is about 1/1000th that of galaxies with the same  $M_{\text{HI}}$  (see also Briggs 1990). Other known tidal HI clouds such as those near NGC 3263 (HIPASS J1029–44b) and NGC 7582 (HIPASS J2318–42), see Appendix B.4, are contained in the BGC as part of their associated galaxy or galaxy group.

Therefore, no definite free-floating HI clouds without stars have been discovered in the search volume. Following Fisher & Tully (1981b) we derive an HI density of  $\rho_{\text{HIclouds}} < 5.4 \times 10^5 M_{\odot} \text{ Mpc}^{-3}$  or  $< 3.7 \times 10^{-35} \text{ g cm}^{-3}$  for HI clouds with  $w_{50} = 100 \text{ km s}^{-1}$  and  $M_{\text{HI}} = 10^7 - 10^{10} M_{\odot}$ . We compare the limit for  $\rho_{\text{HIclouds}}$  with the critical density for the closure of the Universe,  $\rho_c$ , the baryonic mass density,  $\rho_b$ , and the HI mass

density of galaxies,  $\rho_{\text{HIG}}$ , (see Zwaan et al. 2003):  $\rho_{\text{HIclouds}}/\rho_{\text{c}} < 3.5 \times 10^{-6}$ ,  $\rho_{\text{HIclouds}}/\rho_{\text{b}} < 9.9 \times 10^{-5}$ ,  $\rho_{\text{HIclouds}}/\rho_{\text{HIG}} < 8.9 \times 10^{-3}$ .

Since radio wavelengths suffer little absorption in the Galactic Plane, HIPASS provides a clear view of the local large-scale structure. The dominant features in the sky distribution of the BGC are the Supergalactic Plane and the Local Void. In addition, one can clearly see the Centaurus Wall which connects via the Hydra and Antlia clusters to the Puppis filament. Some previously hardly noticed galaxy groups stand out quite distinctively in the H I sky distribution. Several new structures can be mapped for the first time, not only behind the Milky Way.

### Acknowledgments

- We are grateful to the staff at the ATNF Parkes and Narrabri observatories for assistance with HIPASS and follow-up observations.
- We thank Jay Ekers for her help with the HIPASS cube making and galaxy finding.
- This research has made use of the NASA / IPAC Extragalactic Database (NED) which is operated by the Jet Propulsion Laboratory, California Institute of Technology, under contract with the National Aeronautics and Space Administration. We also acknowledge extensive use of the Lyon/Meudon Extragalactic Database (LEDA; see <http://leda.univ-lyon1.fr>).
- Digitized Sky Survey (DSS) material (UKST / ROE / AAO / STScI) is acknowledged.

## A. Galaxies with discrepant velocities

The HIPASS BGC contains 16 galaxies where the measured H I velocity disagrees with the first-listed velocity of the likely optical counterpart given in NED (at the time of the optical identification, see Section 3.5). In Table 7 we list the systemic velocities obtained from HIPASS (Col. 2) as well as previous optical and H I velocity measurements collected from the literature. At the discrepant velocities no H I emission was detected in HIPASS unless stated otherwise.

ATCA H I follow-up observations have confirmed the optical positions and H I velocities obtained for HIPASS J0312-21 (ESO547-G019) and HIPASS J1051-34 (ESO376-G022, see Fig 27). In those cases where the HIPASS and optical velocities cannot be reconciled (e.g. ESO172-G004, ESO173-G016) we conclude that either the published optical velocity is in error or, in a few cases, the field may contain two galaxies: e.g., one uncataloged H I-rich LSB galaxy and one cataloged H I-poor galaxy. In two cases (ESO221-G006, ESO138-G009) previously published H I velocities are substantially offset from the HIPASS velocity. For the galaxy "pair" ESO252-IG001 ATCA H I observations have confirmed that HIPASS J0457-42 is the western, more face-on galaxy ( $PA = 45^\circ$ ). The optical velocities (see Table 7) probably refer to the more distant, nearly edge-on, eastern galaxy, which was also detected in HIPASS and contains a small amount of H I gas at velocities of 2800–3000  $\text{km s}^{-1}$ . Further ATCA H I follow-up observations of BGC sources are under way to provide the correct identifications.

## B. Individual Galaxies in the BGC

### B.1. Extended galaxies

Here we give a brief description of all extended sources in the BGC (see Table 5):

- The Sculptor Group is so close that the largest of its members are resolved with the Parkes telescope: NGC 55 (HIPASS J0015-39), NGC 247 (HIPASS J0047-20), NGC 253 (HIPASS J0047-25), NGC 300 (HIPASS J0054-37) and NGC 7793 (HIPASS J2357-32). The integrated H I flux densities obtained from HIPASS are generally consistent with the single dish H I flux densities given in the literature (see Huchtmeier & Richter 1989), although for NGC 55 and NGC 253 they vary by a factor of two, and are always higher (as expected) than previous VLA measurements (see Puche & Carignan 1991, and references therein). The blue-shifted velocities of some Sculptor Group galaxies

are confused by Galactic H I emission and H I clouds in the Magellanic Stream (see also Putman et al. 2003), which slightly increases the measurement uncertainties. For the starburst galaxy NGC 253 we measure an integrated H I flux density of  $693 \pm 42 \text{ Jy km s}^{-1}$ ; see Koribalski, Whiteoak & Houghton (1995) for a detailed study.

- NGC 1291 (HIPASS J0317-41) is a large, nearly face-on, early-type spiral galaxy of type SBa. Mebold et al. (1979) and Reif et al. (1982) measured an integrated H I flux density of  $72.5 \pm 5.9 \text{ Jy km s}^{-1}$ , slightly lower than our measurement of  $F_{\text{HI}} = 90 \pm 12 \text{ Jy km s}^{-1}$ . Using VLA H I data van Driel, Rots & van Woerden (1988) show that the H I gas is concentrated in an annulus (diameter  $\gtrsim 10'$ ), extending well beyond the optical bar.
- NGC 1313 (HIPASS J0317-66) is a late-type barred spiral galaxy which has been studied in detail by Ryder et al. (1995) who find a large H I disk extending roughly  $18' \times 10'$  ( $24 \text{ kpc} \times 13 \text{ kpc}$ ). We measure an integrated H I flux density of  $463 \pm 33 \text{ Jy km s}^{-1}$  in agreement with  $F_{\text{HI}} = 484 \text{ Jy km s}^{-1}$  obtained by Ryder et al. (1995).
- HIPASS J0403-43 is an interacting galaxy pair consisting of the lenticular galaxy NGC 1512 and the elliptical galaxy NGC 1510 which are separated by  $5''.0$ . We measure an integrated H I flux density of  $259 \pm 17 \text{ Jy km s}^{-1}$  and a deconvolved H I diameter of  $17.4 \times 10.7$  ( $48 \text{ kpc} \times 30 \text{ kpc}$ ). The H I emission is centered on NGC 1512. Hawarden et al. (1979) measure  $F_{\text{HI}} = 232 \pm 20 \text{ Jy km s}^{-1}$  (same as Reif et al. 1982) and a deconvolved H I diameter of  $17' \times 15'$  ( $47 \text{ kpc} \times 41 \text{ kpc}$ ).
- NGC 1533 (HIPASS J0409-56) is a nearby, early-type galaxy with two small companions, IC 2038/9. We measure an integrated H I flux density of  $68 \pm 8 \text{ Jy km s}^{-1}$ , slightly smaller than  $F_{\text{HI}} = 87.5 \pm 6.5 \text{ Jy km s}^{-1}$  by Reif et al. (1982). Recent ATCA H I observations obtained by Ryan-Weber, Webster & Staveley-Smith (2003) reveal an asymmetric H I ring surrounding the optical galaxy with an extent of  $\sim 15'$ . Only a small amount of H I gas is associated with the galaxy IC 2038, none with IC 2039.
- NGC 1532 (HIPASS J0411-32) is a large spiral galaxy interacting with its much smaller, elliptical companion NGC 1531. VLA H I measurements of NGC 1531/2 by Sandage & Fomalont (1993) reveal a total H I extent of  $\sim 20'$  ( $\sim 70 \text{ kpc}$ ) and an integrated H I flux density of  $228 \pm 15 \text{ Jy km s}^{-1}$ , similar to our value of  $249 \pm 15 \text{ Jy km s}^{-1}$ . For a study of the CO(1-0) and CO(2-1) content of NGC 1532 see Horellou et al. (1995).
- NGC 2915 (HIPASS J0926-76) is a weak blue compact dwarf galaxy with a very extended H I disk revealing a short central bar and extended spiral arms extending well beyond the stellar distribution. Using the AT Compact Array Meurer et al. (1996) obtained an integrated H I flux density of  $145 \text{ Jy km s}^{-1}$  and an H I diameter of nearly  $20'$ , which corresponds to five times its Holmberg radius. Our measurement of the integrated flux density,  $F_{\text{HI}} = 108 \pm 14 \text{ Jy km s}^{-1}$ , is significantly lower, and a Gaussian fit to the H I distribution from HIPASS gives a diameter of only  $\sim 9'$  ( $7 \text{ kpc}$ ). Both are underestimates due to strong negative sidelobes.
- NGC 3109 (DDO 236, HIPASS J1003-26A) is a Magellanic-type spiral galaxy. With a distance of 1.25 Mpc (Mateo 1998) it lies at the outskirts of the Local Group. We measure an H I diameter of  $23' \times 6'$  ( $8 \text{ kpc} \times 2 \text{ kpc}$ ) and an integrated H I flux density of  $F_{\text{HI}} = 1148 \pm 97 \text{ Jy km s}^{-1}$ . The resulting H I mass of  $4.2 \times 10^8 M_\odot$  agrees well with that by Barnes & de Blok (2001).

Using the 21-cm multibeam system on the Parkes telescope and narrow-band filters Barnes & de Blok (2001) acquired a deep H I image of NGC 3109 and its neighbour, the Antlia dwarf galaxy. They measure an H I extent of  $\sim 18'$  for NGC 3109.

- NGC 3621 (HIPASS J1118–32) is a nearby spiral galaxy with an optical diameter of about  $12' \times 7'$ . Our integrated H I flux density measurement of  $F_{\text{HI}} = 884 \pm 56 \text{ Jy km s}^{-1}$  compares well with the previous estimate of  $846 \text{ Jy km s}^{-1}$  (see Huchtmeier & Richter 1989). We determine an H I diameter of  $19' \times 4'$  ( $34 \text{ kpc} \times 7 \text{ kpc}$ ). A deep ATCA H I image obtained by Ryan-Weber (priv. comm.) shows a total H I extent of  $32' \times 11'$  ( $58 \text{ kpc} \times 20 \text{ kpc}$ ). The cepheid distance of NGC 3621 is 6.6 Mpc (Willick & Batra 2001), compared to 6.2 Mpc adopted here.
- NGC 4945 (HIPASS J1305–49) is an edge-on starburst galaxy with an H I extent of  $\sim 20'$  ( $\sim 25 \text{ kpc}$ ). We measure an integrated H I flux density of  $F_{\text{HI}} = 319 \pm 21 \text{ Jy km s}^{-1}$ . The ATCA measurement of  $F_{\text{HI}} = 70 \text{ Jy km s}^{-1}$  by Ott et al. (2001) is severely affected by H I absorption. Mathewson & Ford (1996) measure  $F_{\text{HI}} = 269 \text{ Jy km s}^{-1}$ .
- For a detailed discussion of NGC 5128 (Centaurus A, HIPASS J1324–42) see Section 3.6.
- NGC 5236 (M 83, HIPASS J0317–41) is a nearly face-on, gas-rich spiral galaxy located within a loose group of galaxies (see Fig. 28). We measure an integrated H I flux density of  $1630 \pm 96 \text{ Jy km s}^{-1}$  and a deconvolved Gaussian H I diameter of  $31'.2 \times 21'.4$  ( $40 \text{ kpc} \times 28 \text{ kpc}$ ). Huchtmeier & Bohnenstengel (1981) measure a maximum H I extent of  $95' \times 76'$ . Park et al. (2001) obtained a large H I mosaic with the ATCA and Parkes showing an extent of at least  $60'$ . The dwarf companions NGC 5253 (HIPASS J1339–31A) and NGC 5264 (HIPASS J1341–29) lie at projected distances of  $113'$  and  $60'$  from NGC 5236, respectively (see also Banks et al. 1999 and Koribalski 2002).
- The Circinus galaxy (HIPASS J1413–65) is a large bright galaxy at low Galactic latitude ( $b = -4^\circ$ ); for a detailed study see Freeman et al. (1977) and Jones et al. (1999). We find the H I diameter to be about twice its Holmberg diameter. Freeman et al. (1977) and Henning et al. (2000) find integrated H I flux densities of 1907 and  $1867 \text{ Jy km s}^{-1}$ , respectively, significantly larger than our value of  $F_{\text{HI}} = 1451 \pm 98 \text{ Jy km s}^{-1}$  which is an underestimate due to strong negative side-lobes.
- HIPASS J1532–56 (HIZSS 097, HIZOA J1532–56) was discovered by Staveley-Smith et al. (1998) as one of the most extended ( $\leq 200 \text{ kpc}$ ) sources in the H I survey of the Zone of Avoidance (see also Henning et al. 2000, Juraszek et al. 2000). ATCA H I observations by Staveley-Smith et al. (1998) reveal an irregular gas distribution and complex velocity field suggesting this source is an interacting galaxy group, similar to the M 81/M 82/NGC 3077 group (Yun, Ho & Lo 1994). At a location close to zero degrees latitude the Galactic extinction is so large that no optical or infrared identifications have been possible. Our measurement of the integrated H I flux density of J1532–56 ( $F_{\text{HI}} = 64 \pm 15 \text{ Jy km s}^{-1}$ ) is up to a factor of two higher than previous values.
- HIPASS J1616–55 (HIZSS 102, HIZOA J1616–55) was also discovered by Staveley-Smith et al. (1998) who measure a total H I extent of  $80'$ . ATCA H I observations reveal numerous clumps, but no optical counterpart has been found. While this could be a pair of interacting low-surface brightness galaxies, as suggested

by Staveley-Smith et al., we believe it is one of several extended H I clouds representing tidal debris related to the Magellanic Clouds and the Leading Arm (Putman et al. 1998). Our measurement of the integrated H I flux density of J1616–55 ( $F_{\text{HI}} = 24 \pm 7 \text{ Jy km s}^{-1}$ ) is similar to previous values.

- HIPASS J1718–59 was discovered by Koribalski (2001) and has an H I extent of  $\sim 3^\circ$ . No optical counterpart has been identified and we believe this to be another extended H I cloud. It lies only a few degrees away from HIPASS J1712–64 and at a similar velocity to HIPASS J1616–55. The H I properties of the clouds are also listed in Table 4.
- NGC 6744 (HIPASS J1909–63a) is one of the largest galaxies in the southern sky. Using ATCA data Ryder, Walsh & Malin (1999) measure a total H I extent of  $\sim 30'$ , about 1.5 times the size of the stellar disk. The two late-type dwarf companions, NGC 6744A (located within the H I disk of NGC 6744) and ESO104-G044 (HIPASS J1911–64, at a projected distance of  $24'.2$  from NGC 6744) also contain H I gas. We derive an H I mass of  $2.2 \times 10^{10} M_\odot$ , making NGC 6744 one of the most massive galaxies within a distance of  $\sim 25 \text{ Mpc}$ .
- HIPASS J1943–06 is a nearby, possibly interacting galaxy pair ( $F_{\text{HI}} = 45 \pm 7 \text{ Jy km s}^{-1}$ ). It consists of the two galaxies, MCG-01-50-001 and NGC 6821 (MCG-01-50-002), which have nearly identical systemic velocities and are separated by  $18'.9$ . The HIPASS data show a common H I envelope, but interferometric H I observations are needed to study this gas-rich galaxy pair in detail. By fitting two Gaussians to the integrated H I distribution we obtain  $F_{\text{HI}} = 20.4$  and  $24.2 \text{ Jy km s}^{-1}$  for MCG-01-50-001 and NGC 6821, respectively.
- NGC 6822 (HIPASS J1944–14) is, with a distance of 490 kpc (Mateo 1998), the most nearby dwarf irregular galaxy beyond the satellites of the Milky Way. Our measurement of  $F_{\text{HI}} = 2525 \pm 250 \text{ Jy km s}^{-1}$  is slightly contaminated by Galactic emission. Using extensive ATCA observations de Blok & Walter (2000) measure  $F_{\text{HI}} = 2200 \pm 100 \text{ Jy km s}^{-1}$  and a total H I extent of  $40'$ .
- HIPASS J2318–42 is a compact interacting galaxy group consisting of the gas-rich spiral galaxies NGC 7582, NGC 7590 and NGC 7599. These form, together with NGC 7552 (= HIPASS J2316–42), the Grus Quartet. All four galaxies have large amounts of H I gas. ATCA H I observations show tidal tails emanating from NGC 7852 towards NGC 7890/9 and NGC 7552 (see Koribalski 1996).

## B.2. Some Local Group galaxies

Here we describe some of the Local Group galaxies detected in the BGC (NGC 3109 and NGC 6822 have already been described in the previous Section).

- The Wolf-Lundmark Melotte (DDO 221, HIPASS J0001–15) is a Local Group dwarf irregular galaxy at a distance of  $\sim 900 \text{ kpc}$  (Mateo 1998, Dolphin 2000, Rejkuba et al. 2000). Despite its large optical diameter of  $12' \times 4'$  it appears unresolved in HIPASS. However, using Effelsberg H I data Huchtmeier, Seiradakis & Materne (1981) find a total H I extent of  $45'$  ( $12 \text{ kpc}$ ) and an H I mass of  $5.3 \times 10^7 M_\odot$ . We obtained a lower value of  $M_{\text{HI}} = 4.7 \times 10^7 M_\odot$ . Note that the WLM is, in projection, located just north-east of the Magellanic Stream.

- Sextans A (HIPASS J1010–04) is another Local Group dwarf irregular galaxy at a distance of 1.44 Mpc (Mateo 1998). Huchtmeier, Seiradakis, & Materne (1981) reported an H I diameter of 54′ ( $\sim 23$  kpc), 5.8 times the Holmberg diameter, and an H I mass of  $1.3 \times 10^8 M_{\odot}$ . We derive a lower H I mass of  $8.2 \times 10^7 M_{\odot}$ . Wilcots & Hunter (2002) obtained an H I mosaic of Sextans A using the VLA and measured an H I diameter of only 18′ ( $\sim 8$  kpc) and  $M_{\text{HI}} = 8 \times 10^7 M_{\odot}$  (see also Skillman et al. 1988). Sextans A appears unresolved in HIPASS. — The linear separation between Sextans A and NGC 3109 (see above) is only  $\sim 500$  kpc. Together with Antlia and Sextans B this small group may be the closest external clustering of galaxies (van den Bergh 1999).
- IC 5152 (HIPASS J2202–51) is a dwarf irregular galaxy at a distance of 1.59 Mpc (Mateo 1998) with an optical diameter of  $\sim 5'$ . Our value of  $F_{\text{HI}} = 97 \pm 10 \text{ Jy km s}^{-1}$  agrees with that by Huchtmeier & Richter (1986) and results in an H I mass of  $5.8 \times 10^7 M_{\odot}$ . Zijlstra & Minniti (1999) determine a similar distance of 1.7 Mpc.
- HIPASS J0700–04 (HIZSS 003, Henning et al. 2000) is the closest newly cataloged galaxy in the BGC with  $v_{\text{LG}} = 115 \text{ km s}^{-1}$ . Recent observations by Massey, Henning & Kraan-Korteweg (2003) show it to be a regularly rotating, dwarf irregular galaxy with an H I extent of 6′.

### B.3. Galaxies with the highest HI mass

The BGC sources with the highest H I masses are ESO390-G004 and NGC 5291, followed by the galaxy pair NGC 6935/7 and the barred spiral galaxy ESO136-G016.

- ESO390-G004 (HIPASS J1620–36) lies close to the Zone of Avoidance ( $b = 9^{\circ}8$ ,  $A_{\text{B}} = 3.1$  mag); no optical velocity is available. Theureau et al. (1998) measure a systemic velocity of  $4448 \pm 6 \text{ km s}^{-1}$ , in agreement with our measurement, but an integrated H I flux density of only  $23.7 \pm 2.0 \text{ Jy km s}^{-1}$  using the Nançay telescope. Although the HIPASS spectrum is affected by some baseline ripple, our measurement of  $F_{\text{HI}} = 47 \pm 6 \text{ Jy km s}^{-1}$  is reliable. Optically the galaxy shows a bright core plus some extended emission. We estimate an H I mass of  $3.7 \times 10^{10} M_{\odot}$ . Preliminary ATCA H I snapshot observations show that there is at least one uncataloged companion,  $\sim 2'$  SE of ESO390-G004, which contributes to the  $F_{\text{HI}}$  measurement. The  $F_{\text{HI}}$  discrepancy between the Parkes and Nançay measurements may be explained by the different beam sizes of the telescopes.
- The peculiar system NGC 5291 (HIPASS J1347–30), located in the western outskirts of the cluster Abell 3574, contains the lenticular galaxy NGC 5291 and a close companion, the so-called ‘Seashell’ galaxy, as well as numerous bright knots (see e.g. Duc & Mirabel 1998). One of these knots is classified as the H II galaxy CTS1032 ( $v_{\text{opt}} = 4350 \pm 99 \text{ km s}^{-1}$ , Pena, Ruiz & Maza 1991). Malphrus et al. (1997) find an unusually high amount of H I gas distributed along a fragmented ring of diameter  $9'9$  (NS)  $\times$   $5'6$  (EW), covering NGC 5291, the ‘Seashell’ galaxy, CTS1032, and at least another 10 knots. The 20% velocity width of the NGC 5291 system is the largest measured in the BGC ( $w_{50} = 637 \text{ km s}^{-1}$ ,  $w_{20} = 757 \text{ km s}^{-1}$ ). Longmore et al. (1979) measured a single dish H I mass of  $5 \times 10^{10} M_{\odot}$ , assuming  $D = 58$  Mpc. Our measurement of  $M_{\text{HI}} = 3.6 \times 10^{10} M_{\odot}$  ( $D = 56$  Mpc) is similar.
- HIPASS J2038–52 corresponds to the galaxy pair NGC 6935/7 (separation 4'5). ATCA H I snapshot

observations show another small galaxy possibly contributing to the H I emission. This new galaxy lies  $\sim 6'$  to the NNW of the early-type galaxy NGC 6935. The H I emission appears to be dominated by the spiral galaxy NGC 6937 for which Huchtmeier & Richter (1989) quote an integrated flux density of  $31.8 \pm 4.1 \text{ Jy km s}^{-1}$ , close to our measurement of  $33.1 \text{ Jy km s}^{-1}$ . The H I mass of the system is  $3.1 \times 10^{10} M_{\odot}$ .

- ESO136-G016 (HIPASS J1603–60) is a distant edge-on, barred spiral galaxy. At a latitude of  $b = -6^{\circ}3$  and  $A_{\text{B}} = 1.4$  mag, it appears very faint in the DSS 1, but is clearly visible on red DSS 2 images. Its optical diameter is about 3'5, no optical velocity is available. Our measurement of  $F_{\text{HI}} = 25.5 \pm 3.7 \text{ Jy km s}^{-1}$  agrees well with the previous estimate of  $27.40 \pm 4.1 \text{ Jy km s}^{-1}$  (Huchtmeier & Richter 1989). We derive an H I mass of  $3.0 \times 10^{10} M_{\odot}$ . ATCA H I observations are needed to study the neighbourhood and gas kinematics in detail. The red DSS 2 image shows a potential companion a few arcminutes to the north-west.

### B.4. Galaxies with the largest HI velocity widths

The BGC sources with the largest measured 50% velocity widths are NGC 5084, NGC 5291 (see above) and NGC 2613.

- NGC 5084 (HIPASS J1320–21) is a massive and unusual lenticular galaxy (see Gottesman & Hawarden 1986). It has a radius of 8'2 ( $\sim 50$  kpc) and is close to edge-on ( $i > 86^{\circ}$ ). We measure  $F_{\text{HI}} = 101.5 \pm 6.7 \text{ Jy km s}^{-1}$ ,  $w_{50} = 645 \text{ km s}^{-1}$ , and  $w_{20} = 668 \text{ km s}^{-1}$ . Using  $v_{\text{rot}} = w_{20} / 2$  we estimate a total dynamical mass of  $M_{\text{tot}} = 1.3 \times 10^{12} M_{\odot}$ , and a mass-to-light ratio  $\gtrsim 65$ . At a slightly higher velocity and a projected distance of 15' lies the companion galaxy ESO576-G040 (HIPASS J1320–22), also a member of the BGC. The total dynamical mass is derived using  $M_{\text{tot}} [M_{\odot}] = 2.31 \times 10^5 r_{\text{kpc}} v_{\text{rot}}^2$ , where  $v_{\text{rot}}$  is the inclination corrected rotation velocity of the galaxy in  $\text{km s}^{-1}$  and  $r_{\text{kpc}}$  is the galaxy radius.
- NGC 2613 (HIPASS J0833–22) is a bright Sb galaxy with an optical radius of 3'6 and an inclination of  $76^{\circ}$ . We measure an integrated H I flux density of  $59.4 \pm 4.6 \text{ Jy km s}^{-1}$ ,  $w_{50} = 602 \text{ km s}^{-1}$ , and  $w_{20} = 620 \text{ km s}^{-1}$ . Using WSRT data, Bottema (1989) measured a much lower H I flux of  $29.4 \text{ Jy km s}^{-1}$  and derived a rotation velocity of  $315 \text{ km s}^{-1}$ . Chaves & Irwin (2001) used the VLA to image NGC 2613 and its companion, ESO495-G017, and measured integrated H I flux densities of  $55.2 \text{ Jy km s}^{-1}$  and  $1.6 \text{ Jy km s}^{-1}$ , respectively. Using their H I radius of  $\sim 5'$  ( $\sim 27$  kpc) we derive a total dynamical mass of  $M_{\text{tot}} \sim 6 \times 10^{11} M_{\odot}$  for NGC 2613. The small companion galaxy, ESO495-G017, lies at a projected distance of 7'3.

The largest 20% velocity widths were measured in NGC 5291 and NGC 5084, followed by NGC 5183/4, ESO320-G026 and NGC 3263.

- The spiral galaxies NGC 5183/4 (HIPASS J1330–01;  $F_{\text{HI}} = 29.2 \pm 3.0 \text{ Jy km s}^{-1}$ ) are separated by only 3'7. We measure velocity widths of  $w_{50} = 346 \text{ km s}^{-1}$  and  $w_{20} = 666 \text{ km s}^{-1}$ . Huchtmeier & Richter (1989) give integrated H I flux densities of  $17.3$  and  $10.9 \text{ Jy km s}^{-1}$ , respectively. The individual galaxies have velocity widths of only  $\sim 360 \text{ km s}^{-1}$  (de Vaucouleurs et al. 1991).

- The Sb galaxy ESO320-G026 (HIPASS J1149–38) is confused by the smaller spiral ESO320-G024, which lies at a projected distance of 6'. We measure  $F_{\text{HI}} = 37.2 \pm 4.3 \text{ Jy km s}^{-1}$ ,  $w_{50} = 329 \text{ km s}^{-1}$ , and  $w_{20} = 641 \text{ km s}^{-1}$ . Neither galaxy has previous HI measurements.
- NGC 3263 (HIPASS J1029–44b) is a peculiar galaxy and part of a group of HI rich galaxies (Koribalski et al. 2004, in prep.). Best known in this loose group is the galaxy merger NGC 3256 (HIPASS J1027–43) which exhibits a spectacular set of symmetric tidal arms both in the optical and in HI. A large HI gas cloud to the west of NGC 3263 (English, Koribalski & Freeman 2003) as well as the galaxy NGC 3261 (HIPASS J1029–44a) also contribute to the integrated HI flux density. We measure  $F_{\text{HI}} = 79.1 \pm 5.6 \text{ Jy km s}^{-1}$ ,  $w_{50} = 423 \text{ km s}^{-1}$ , and  $w_{20} = 630 \text{ km s}^{-1}$ .

None of these galaxies compares with the S0/Sa galaxy UGC 12591 which appears to have one of the largest rotational velocity ( $w_{50} = 957 \text{ km s}^{-1}$ ) of any known disk system (Giovanelli et al. 1986). We note that LEDA lists velocity widths larger than  $700 \text{ km s}^{-1}$  ( $800 \text{ km s}^{-1}$ ) for 17 (6) galaxy systems.

## REFERENCES

- Baars, J.W.M., Genzel, R., Pauliny-Toth, I.I., Witzel, A. 1977, A&A 61, 99
- Baldwin, J.E., Lynden-Bell, D., Sancisi, R. 1980, MNRAS 193, 313
- Banks, G.D., Disney, M.J., Knezek, P.M., *et al.* 1999, ApJ 524, 612
- Barnes, J.E., Hernquist, L. 1992, Nature 360, 715
- Barnes, D.G., de Blok, W.J.G. 2001, AJ 122, 825
- Barnes, D.G., Staveley-Smith, L., de Blok, W.J.G., *et al.* 2001, MNRAS 322, 486
- de Blok, W.J.G., Walter, F. 2000, ApJ 537, L95
- Bothun, G.D., Schombert, J.M., Impey, C.D., Sprayberry, D., McGaugh, S. S. 1993, AJ 106, 530
- Bottema, R. 1989, A&A 225, 358
- Bottinelli, L., Gouguenheim, L., Fouqué, P., Paturel, G. 1990, A&AS 82, 391
- Boyce, P.J., Minchin, R.F., Kilborn, V.A., Disney, M.J., Lang, R.H., Jordan, C.A., Grossi, M., Lyne, A.G.R., Cohen, R.J., Morison, I.M., Phillipps, S. 2001, ApJ 560, L127
- Braine, J., Duc, P.-A., Lisenfeld, U., Charmandaris, V., Vallejo, O., Leon, S., Brinks, E. 2001, A&A 378, 51
- Briggs, F.H. 1990, AJ 100, 999
- Briggs, F.H. 1997, ApJ 484, L29
- Broeils, A.H., van Woerden, H. 1994, A&AS 107, 129
- Broeils, A.H., Rhee, M.-H. 1997, A&A 324, 877
- Chaves, T.A., Irwin, J.A. 2001, ApJ 557, 646
- Chengalur, J.N., Giovanelli, R., Haynes, M.P. 1995, AJ 109, 2415
- Coté, S., Freeman, K., Carignan, C., Quinn, P.J. 1997, AJ 114, 1313
- Da Costa, L.N., Pellegrini, P.S., Davis, M., Meiksin, A., Sargent, W.L.W., Tonry, J.L. 1991, ApJS 75, 935
- van den Bergh, S. 1999, ApJ 517, L97
- van den Bergh, S. 2000, PASP 112, 529
- Dolphin, A.E. 2000, ApJ 531, 804
- Dressler A. 1991, ApJS 75, 241
- van Driel, W., Rots, A.H., van Woerden, H. 1988, A&A 204, 39
- Duc, P.-A., Mirabel, I.F. 1997, The Messenger, 89, 14
- Duc, P.-A., Mirabel, I.F. 1998, A&A 333, 813
- Duc, P.-A., Brinks, E., Springel, V., Pichardo, B., Weilbacher, P., Mirabel, I.F. 2000, AJ 120, 1238
- Duprie, K., Schneider, S.E. 1996, AJ 112, 937
- Efstathiou, G.P., Ellis, R.S., Peterson, B.A. 1988, MNRAS 232, 431
- English, J., Koribalski, B.S., Freeman, K.C. 2003, in ‘Recycling Interstellar and Intergalactic Matter’, IAU Symposium No 217, eds. P.A. Duc, J. Braine, and E. Brinks, in press
- Ellison, S.L., Yan, L., Hook, I.M., Pettini, M., Wall, J.V., Shaver, P. 2002, A&A 379, 393

- Faber, S.M., Burstein D. 1988, in Proc. of the Vatican Study Week, Large-Scale Motions in the Universe”, eds. V.C. Rubin & G.V. Coyne, Princeton University Press, p. 115
- Fairall, A.P. 1980, MNRAS 192, 389
- Fairall, A.P. 1998, Large-Scale Structures in the Universe, Chichester, Praxis Publishing Ltd.
- Fairall, A.P., Vettolani G., Chincarini G. 1989, A&AS 78, 269
- Fairall, A.P., Palumbo, G.G.C., Vettolani, G., Kauffmann, G., Jones, A., Baiesi-Pillastrini, G. 1990, MNRAS 247, 21
- Fairall, A., Jones, A. 1991, Southern Redshifts catalog, Publications of the Department of Astronomy, University of Cape Town
- Fairall, A., Woudt P.A., Kraan-Korteweg R.C. 1998, A&AS 127, 463
- Fisher, J.R., Tully, R.B. 1981a, ApJS 47, 139
- Fisher, J.R., Tully, R.B. 1981b, ApJ 243, L23
- Fouqué, P., Durand, N., Bottinelli, L., Gougouenheim, L., Paturel, G. 1990a, A&AS 86, 473
- Fouqué, P., Bottinelli, L., Gougouenheim, L., Paturel, G. 1990b, ApJ 349, 1
- Freeman, K.C., *et al.* 1977, A&A 55, 445
- Gardner, F.F., Whiteoak, J.B. 1976, Proc Astron. Soc. Australia 3, 63
- Geller, M.J., Huchra, J.P. 1989, Science 246, 897
- Giovanelli, R., & Haynes, M.P. 1989, ApJ 346, L5
- Giovanelli, R., & Haynes, M.P. 1990, in “Galactic and Extragalactic Radio Astronomy”, eds. G.L. Verschuur, K.I. Kellermann, p. 522
- Giovanelli, R., Haynes, M.P., Rubin, V.C., Ford, W.K., Jr. 1986, ApJ 301, L7
- Giuricin, G., Samurovic, S., Girardi, M., Mezzetti, M., Marinoni, C. 2001, ApJ 554, 857
- van Gorkom, J.H., van der Hulst, J.M., Haschick, A.D., Tubbs, A.D. 1990, AJ 99, 1781
- Gottesman, S.T., Hawarden, T.G. 1986, MNRAS 219, 759
- Hagiwara, Y., Kohno, K., Kawabe, R., Nakai, N. 1997, PASJ 49, 171
- Hawarden, T.G., van Woerden, H., Goss, W.M., Mebold, U., Peterson, B.A. 1979, A&A 76, 230
- Haynes, M.P., Giovanelli, R., Chincarini, G.L. 1984, ARA&A 22, 445
- Haynes, M.P., Giovanelli, R., Herter, T., Vogt, N.P., Freudling, W., Maia, M.A.G., Salzer, J.J., Wegner, G. 1997, AJ 113, 1197
- Haynes, M.P., Hogg, D.E., Maddalena, R.J., Roberts, M.S., van Zee, L. 1998, AJ 115, 62
- Haynes, M.P., Giovanelli, R., Chamaraux, P., da Costa, L.N., Freudling, W., Salzer, J.J., Wegner, G. 1999, AJ 117, 2039
- Henning, P.A. 1995, ApJ 450, 578
- Henning, P.A., Staveley-Smith, L., Ekers, R.D., *et al.* 2000, AJ 119, 2686
- Hibbard, J.E., van Gorkom, J.H. 1996, AJ 111, 655
- Hibbard, J.E., van der Hulst, J.M., Barnes, J.E., Rich, R.M. 2001, AJ 122, 2969
- Hopp, U., Materne, J. 1985, A&AS 61, 93
- Horellou, C., Casoli, F., Dupraz, C. 1995, A&A 303, 361
- Huchra J.P., Geller M.J., Clemens C.M., Tokarz S.P. and Michel A. 1995, Harvard Smithsonian Center for Astrophysics (The CFA redshift catalog)
- Huchtmeier, W.K., Bohnenstengel, H.-D. 1981, A&A 100, 72
- Huchtmeier, W.K., Richter, O.-G., 1986, A&AS 63, 323
- Huchtmeier, W.K., Richter, O.-G., 1989, A General Catalog of HI Observations of Galaxies, Springer-Verlag
- Huchtmeier, W.K., Seiradakis, J.H., Materne, J. 1980, A&A 91, 341
- Huchtmeier, W.K., Seiradakis, J.H., Materne, J. 1981, A&A 102, 134

- Hui, X., Ford, H.C., Ciardullo, R., Jacoby, G.H. 1993, ApJ 414, 463
- Impey, C.D., Sprayberry, D., Irwin, M.J., Bothun, G.D. 1996, ApJS 105, 209
- Impey, C.D., & Bothun, G.D. 1997, ARA&A 35, 267
- Jarrett, T.H., Chester T., Cutri, R., Schneider, S.E., Huchra, J.P. 2003, AJ 125, 525
- Juraszek, S.J., Staveley-Smith, L., Kraan-Korteweg, R.C. *et al.* 2000, AJ 119, 1627
- Jones, K.L., Koribalski, B.S., Elmouttie, M., Haynes, R.F. 1999, MNRAS 302, 649
- Karachentsev, I.D., et al. 2003, A&A 398, 479
- Kerr, F.J., & Henning, P.A. 1987, ApJ 320, L99
- Kilborn, V.A. 2001, PhD Thesis, University of Melbourne
- Kilborn, V.A., Staveley-Smith, L., Marquarding, M., *et al.* 2000, AJ 120, 1342
- Kilborn, V.A., Webster, R.L., Staveley-Smith, L., *et al.* 2002, AJ 124, 690
- Koribalski, B.S., Whiteoak, J.B., Houghton, S. 1995, PASA 12, 20
- Koribalski, B.S. 1996, in “The Minnesota Lectures on Extragalactic Neutral Hydrogen”, ASP Conf. Series Vol. 106, ed. E.D. Skillman, p. 238
- Koribalski, B.S. 2001, in “Gas and Galaxy Evolution”, ASP Conf. Ser. Vol. 240, eds. J. E. Hibbard, M. P. Rupen & J. H. van Gorkom, San Francisco, p. 439
- Koribalski, B.S. 2002, in “Seeing Through the Dust”, ASP Conf. Ser. Vol. 276, eds. A. R. Taylor, T. L. Landecker & A. G. Willis, p. 72
- Koribalski, B.S., Dickey, J.M. 2004, MNRAS 348, 1255
- Kraan-Korteweg, R.C., Lahav, O. 2000, A&ARv 10, 211
- Lahav, O., Santiago, B.X., Webster, A.M., Strauss, M.A., Davis, M., Dressler, A., Huchra, J.P. 2000, MNRAS 312, 166
- Lane, W.M., Clarke, T.E., Taylor, G.B., Perley, R.A., Kassim, N.E. 2004, AJ 127, 48
- Lang, R.H., et al. 2003, MNRAS 342, 738
- Lauberts, A. 1982, ESO/Uppsala survey of the ESO(B) atlas
- Lauberts, A., Valentijn, E.A. 1989, The Surface Photometry Catalogue of the ESO/Uppsala galaxies, Garching bei München, ESO
- Lewis, G.F., Irwin, M.J., Ibata, R.A., Gibson, B.K. 2002, PASA 19, 257
- Longmore, A.J., Hawarden, T.G., Cannon, R.D., Allen, D.A., Mebold, U., Goss, W.M., Reif, K. 1979, MNRAS 188, 285
- Longmore, A.J., Hawarden, T.G., Goss, W.M., Mebold, U., Webster, B.L. 1982, MNRAS 200, 325
- Lynden-Bell, D. 1994, in “Mapping the Hidden Universe”, ASP Conf. Ser. Vol. 67, eds. C. Balkowski & R. C. Kraan-Korteweg, 289
- Lynden-Bell, D., Faber, S.M., Burstein, D., Davies, R.L., Dressler, A., Terlevich, R.J., Wegner, G. 1988, ApJ 326, 19
- Malphrus, B.K., Simpson C.E., Gottesman, S.T., Hawarden, T.G. 1997, AJ 114, 1427
- Massey, P., Henning, P.A., Kraan-Korteweg, R.C. 2003, AJ 126, 2362
- McLin, K.M., Stocke, J.T., Weymann, R.J., Penton, S.V., Shull, J.M. 2002, ApJ 574, L115
- Mateo, M.L. 1998, ARA&A 36, 435
- Mathewson, D.S., Cleary, M.N., Murray, J.D. 1974, ApJ 190, 291
- Mathewson, D.S., Ford, V.L., Buchhorn M. 1992, ApJS 81, 413
- Mathewson, D.S., Ford, V.L. 1996, ApJS 107, 97
- Matthews, L.D., Gallagher, J.S., III., Littleton, J.E. 1995, AJ 110, 581
- Mebold, U., Goss, W.M., van Woerden, H., Hawarden, T.G., Siegman, B. 1979, A&A 74, 100

- Meurer, G.R., Carignan, C., Beaulieu, S.F., Freeman, K.C. 1996, AJ 111, 1551
- Meyer, M.J., *et al.* 2004, MNRAS, accepted
- Nakanishi, K., Takata, T., Yamada, T., Takeuchi, T., Shiroya, R., Miyazawa, M., Watanabe, S., Saito, M. 1997, ApJS 112, 245
- Oosterloo, T.A., Morganti, R., Sadler, E.M., Vergani, D., Caldwell, N. 2002, AJ 123, 729
- Ott, M., Whiteoak, J.B., Henkel, C., Wielebinski, R. 2001, A&A 372, 463
- Park, O.-K., Kalnajs, A. Freeman, K.C., Koribalski, B., Staveley-Smith, L. 2001, in "Galaxy Disks and Disk Galaxies", ASP Conf. Series, Vol. 230, eds. J.G. Funes, E. & M. Corsini, p. 109
- Pei, Y.C., Fall, S.M., Hauser, M.G. 1999, ApJ 522, 604
- Pena, M., Ruiz, M.T., Maza, J. 1991, A&A 251, 417
- Penston, M.V., Fosbury, R.A.E., Ward, M.J., Wilson, A.S. 1977, MNRAS 180, 19
- Penton, S.V., Shull, J.M., Stocke 2000, ApJ 544, 150
- Peterson, B.A., Ellis, R.S., Efstathiou, G., Shanks, T., Bean, A.J., Fong, R., Zen-Long, Z. 1986, MNRAS 221, 233
- Peterson, C.J. 1986, PASP 98, 1273
- Pihlstrom, Y.M., Conway, J.E., Booth, R.S., Diamond, P.J., Koribalski, B.S. 2000, A&A 357, 7
- Puche, D., Carignan, C. 1991, ApJ 378, 487
- Putman, M.E., Gibson, B., Staveley-Smith, L., *et al.* 1998, Nature 394, 752
- Putman, M.E., de Heij, V., Staveley-Smith, L., *et al.* 2002, AJ 123, 873
- Putman, M.E., Staveley-Smith, L., Freeman, K.C., Gibson, B.K., Barnes, D.G. 2003, ApJ 586, 170
- Rao, S., Briggs, F. 1993, ApJ 419, 515
- Rao, S.M., Turnshek, D.A. 2000, ApJS 130, 1
- Reif, K., Mebold, U., Goss, W.M., van Woerden, H., Siegman, B. 1982, A&AS 50, 451
- Rejkuba, M., Minniti, D., Gregg, M.D., Zijlstra, A.A., Alonso, M.V., Goudfrooij, P. 2000, AJ 120, 801
- Richter, O.-G., Sancisi, R. 1994, A&A 290, L9
- Roberts, M.S., Haynes, M.P. 1994, ARA&A 32, 115
- Rosenberg, J.L., Schneider, S.E. 2000, ApJS 130, 177
- Ryan-Weber, E., Koribalski, B., Staveley-Smith, L., *et al.* 2002, AJ 124, 1954
- Ryan-Weber, E.V., Webster, R.L., Staveley-Smith, L. 2003, MNRAS 343, 1195
- Ryder, S.D., Staveley-Smith, L., Malin, D.F., Walsh, W. 1995, AJ 109, 1592
- Ryder, S.D., Walsh, W., Malin, D.F. 1999, PASA 16, 84
- Ryder, S.D., Koribalski, B., Staveley-Smith, L., Kilborn, V.A., Malin, D.F. *et al.* 2001, ApJ 555, 232
- Sadler, E. 2001, in "Gas and Galaxy Evolution", ASP Conf. Ser. Vol. 240, eds. J. E. Hibbard, M. P. Rupen & J. H. van Gorkom, San Francisco, p. 445
- Salpeter, E.E., Hoffman, G.L. 1996, ApJ 465, 595
- Salzer, J.J., Haynes, M.P. 1996, in "The Minnesota Lectures on Extragalactic Neutral Hydrogen", ASP Conf. Series Vol. 106, ed. E.D. Skillman, p. 357
- Sandage, A., Fomalont, E. 1993, ApJ 407, 14
- Saunders, W., Rowan-Robinson, M., Lawrence, A., Efstathiou, G., Kaiser, N., Ellis, R.S., Frenk, C.S. 1990, MNRAS 242, 318
- Schiminovich, D., van Gorkom, J.H., van der Hulst, J.M., Kasow, S. 1994, ApJ 423, L101
- Schneider, S.E. 1989, ApJ 343, 94

- Schneider, S.E. 1996, in “The Minnesota Lectures on Extragalactic Neutral Hydrogen”, ASP Conf. Series Vol. 106, ed. E.D. Skillman, p. 323
- Schneider, S.E., Helou, G., Salpeter, E.E., Terzian, Y. 1986, AJ 92, 742
- Schneider, S.E., Thuan, T.X., Magri, C., Wadiak, J.E. 1990, ApJS 72, 245
- Skillman, E.D., Terlevich, R., Teuben, P.J., van Woerden, H. 1988, A&A 198, 33
- Solanes, J.M., Giovanelli, R., Haynes, M.P. 1996, ApJ 461, 609
- Solanes, J.M., Manrique, A., Garcia-Gómez, C., González-Casado, G., Giovanelli, R., Haynes, M.P. 2001, ApJ 548, 97
- Spitzak, J.G., Schneider, S.E. 1998, ApJS 119, 159
- Stanimirovic, S., Staveley-Smith, L., Dickey, J.M., Sault, R.J., Snowden, S.L. 1999, MNRAS 302, 417
- Staveley-Smith, L., Wilson, W., Bird, T., Disney, M., Ekers, R.D., Freeman, K., Haynes, R., Sinclair, M., Vaile, R., Wright, A. 1996, Publ. ASA 13, 243
- Staveley-Smith, L., Juraszek, S., Koribalski, B., Ekers, R.D., Green, A.J., Haynes, R.F., Henning, P.A., Kesteven, M.J., Kraan-Korteweg, R.C., Price, R.M., Sadler, E.M. 1998, AJ 116, 2727
- Staveley-Smith, L., Kim, S., Calabretta, M.R., Haynes, R.F., Kesteven, M.J. 2003, MNRAS 339, 87
- Storrie-Lombardi, L.J., Wolfe, A.M. 2000, ApJ 543, 552
- Swaters, R.A., van Albada, T.S., van der Hulst, J.M., Sancisi, R. 2002, A&A 390, 829
- Taylor, G.B., Perley, R.A., Inoue, M., Kato, T., Tabara, H., Aizu, K. 1990, ApJ 360, 41
- Theureau, G., *et al.* 1998, A&AS 130, 333
- Tully, R.B. 1982, ApJ 257, 389
- Tully, R.B. 1988, Nearby Galaxies Catalog, Cambridge University Press
- Tully, R.B., Fisher, J.R. 1987, Nearby Galaxies Atlas, Cambridge University Press
- Tully, R.B., Fouqué, P. 1985, ApJS 58, 67
- Turnshek, D.A., Rao, S.M. 2002, ApJ 572, L7
- de Vaucouleurs, G., de Vaucouleurs, A., Corwin, J.R., Buta, R.J., Paturel, G., Fouqué, P. 1991, Third Reference Catalogue of Bright Galaxies, New York, Springer Verlag (RC3)
- Verdes-Montenegro, L., Yun, M.S., Williams, B.A., Huchtmeier, W.K., Del Olmo, A., Perea, J. 2001, A&A 377, 812
- Visvanathan, N., Yamada, T. 1996, ApJS 107, 521
- Waugh, M., Drinkwater, M.J., Webster, R.L., Staveley-Smith, L., Kilborn, V.A. *et al.* 2002, MNRAS 337, 641
- Westerlund, B.E. 1997, ‘The Magellanic Clouds’, Cambridge University Press
- Wilcots, E.M., Hunter, D.A. 2002, AJ 123, 1476
- Willick, J.A., Batra, P. 2001, ApJ 548, 564
- Whiting, A.B., Hau, G.K.T., Irwin M. 2002, ApJS 141, 123
- Young, L.M., Lo, K.Y. 1997, ApJ 490, 710
- Yun, M.S., Ho, P.T.P., Lo K.Y. 1994, Nature 372, 530
- Zijlstra, A.A., Minniti, D. 1999, AJ 117, 1743
- Zwaan, M.A., Briggs, F.H., Sprayberry, D., Sorar, E. 1997, ApJ 490, 173
- Zwaan, M.A., Staveley-Smith, L., Koribalski, B.S. *et al.* 2003, AJ 125, 2842
- Zwaan, M.A., *et al.* 2004, MNRAS, accepted

Fig. 1.— H I spectra of all 1000 members of the HIPASS Bright Galaxy Catalog (BGC). The HIPASS name together with the most likely optical identification (in brackets) is given at the top of each spectrum. Marked are also the measured H I peak flux density as well as the 50% and 20% velocity widths. The vertical lines indicate the velocity range used for the first order baseline fit (outside) and the H I line emission analysis (inside). — The full version of this figure is in the electronic edition of the Journal.

Fig. 1.— continued.

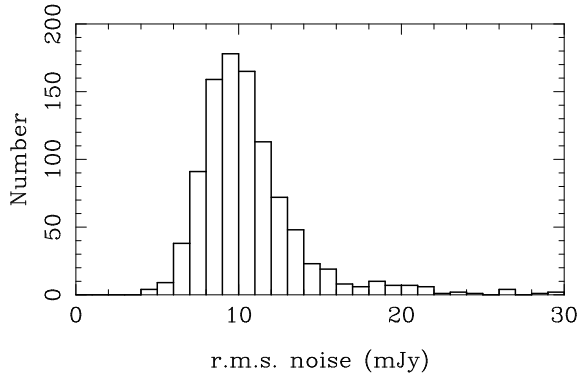


Fig. 2.— Histogram of the clipped r.m.s. of the HIPASS BGC spectra, as determined from the MBSPECT fit of the spatially and spectrally integrated H I spectra. Not displayed here are 24 galaxies with r.m.s.  $>30$  mJy; these are mostly extended sources and some galaxies in the Zone of Avoidance.

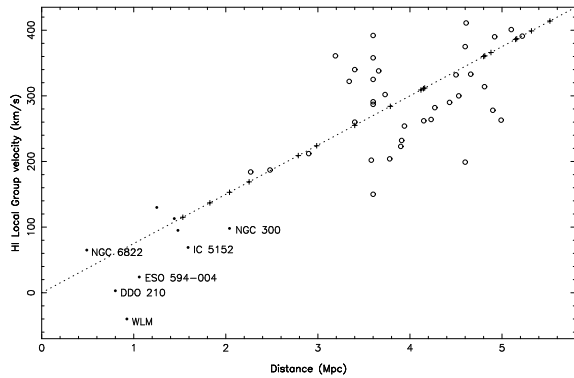


Fig. 3.— Distances versus H I Local Group velocities for the closest galaxies in the BGC. Open and filled circles indicate galaxies for which independent distances are available in the literature (see Section 3.4.2), while the “+” symbols denote the Hubble distance ( $D = v_{\text{LG}} / H_0$ ) for those galaxies for which no independent distances are currently available. The filled circles show those nine galaxies for which the independent distances were adopted in the BGC. The largest deviations occur where one distance is given for members of a galaxy group (e.g., part of the Cen A group at 3.6 Mpc, see Karachentsev et al. 2003).

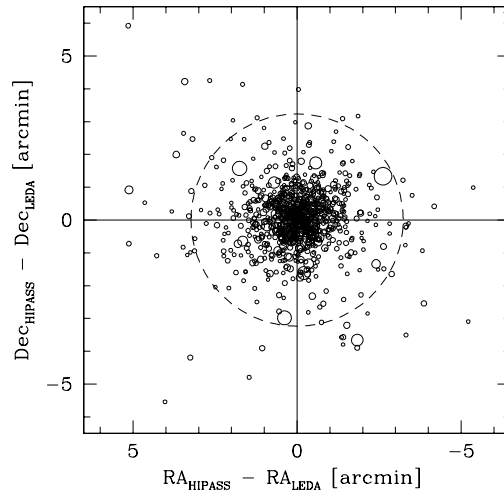


Fig. 4.— The difference between the H I and optical positions of 853 HIPASS BGC objects, using optical positions from LEDA. The remaining 147 BGC members had either no or had multiple optical identifications in LEDA. The dashed circle marks the radius containing 95% of the galaxies at  $3/2$ . The symbol size is proportional to the logarithm of the H I peak flux density.

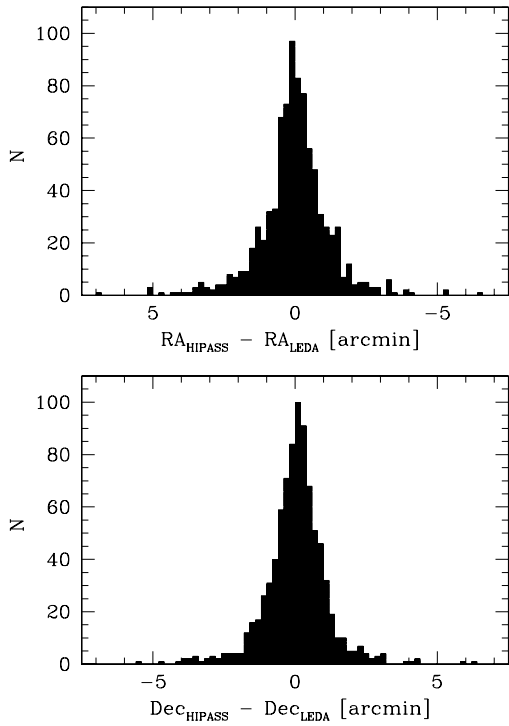


Fig. 5.— Histograms of the difference between the HI and optical Right Ascension (top) and Declination (bottom) values for 853 HIPASS BGC objects.

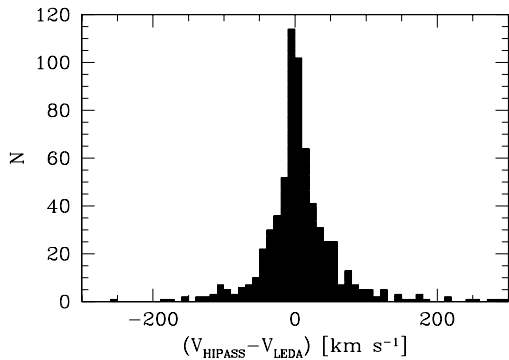


Fig. 6.— Histogram of the difference between the HI and optical systematic velocities for 672 HIPASS BGC objects. For 95% of these galaxies the optical velocities are within  $170 \text{ km s}^{-1}$  of the HIPASS velocities. There are 20 galaxies with differences larger than  $300 \text{ km s}^{-1}$ , these lie outside the velocity range displayed here.

Fig. 7.— Optical DSS image of the field around the nearby galaxy HIPASS J0622–07. The small galaxy CGMW1-0080 was thought to be the optical counterpart of the HI source, but ATCA HI imaging showed that the big galaxy towards the center of the field is the actual counterpart. CGMW1-0080 is likely a background galaxy.

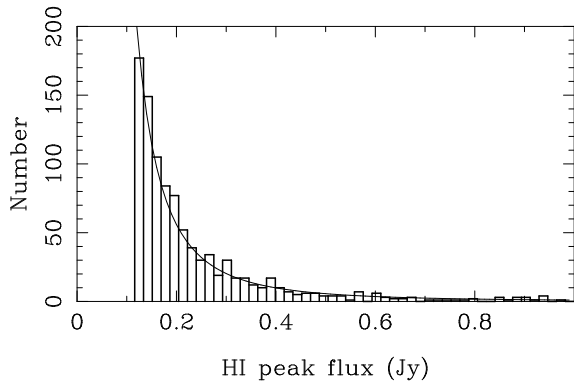


Fig. 8.— Histogram of the measured HI peak flux densities in the HIPASS BGC (the bin size is 20 mJy). The peak flux cutoff at  $S_{\text{peak}} \gtrsim 116 \text{ mJy}$  results from selecting the 1000 HI-brightest galaxies. Not displayed here are 38 galaxies with HI peak flux densities  $>1 \text{ Jy}$ . The overlaid curve is described by  $S_{\text{peak}}^{-2.5}$ , indicating a complete catalog.

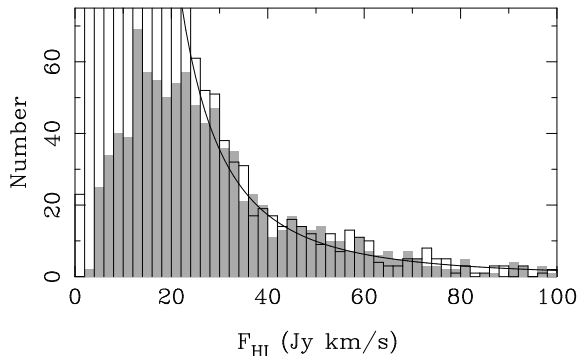


Fig. 9.— Histogram of the integrated HI flux densities ( $F_{\text{HI}}$ ) in the HIPASS BGC (grey) and the HIPASS Catalogue (Meyer et al. 2004). The overlaid curve, which is proportional to  $F_{\text{HI}}^{-2.5}$ , indicates completeness only for BGC sources with  $F_{\text{HI}} \gtrsim 25 \text{ Jy km s}^{-1}$ . Note that the HIPASS Catalogue and the BGC are based on the same survey data, but were compiled and parameterized independently. — About 60 sources with  $F_{\text{HI}} \gtrsim 100 \text{ Jy km s}^{-1}$  are not displayed.

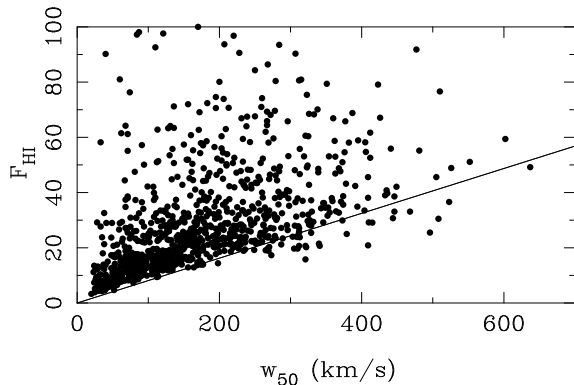


Fig. 10.— Integrated HI flux density,  $F_{\text{HI}}$ , versus the 50% velocity width,  $w_{50}$ . The lower limit to the detectable integrated HI flux density in the HIPASS BGC is approximately given by  $F_{\text{HI}} = 0.7 \times 0.116 w_{50}$  (indicated by the solid line). It applies quite well to galaxies with relatively narrow profiles ( $w_{50} < 250 \text{ km s}^{-1}$ ), but is a factor  $\sim 2$  lower for wide double-horn profiles. Not displayed here are 60 galaxies with  $F_{\text{HI}} \gtrsim 100 \text{ Jy km s}^{-1}$ .

Fig. 11.— Example of strong Galactic recombinations lines in HIPASS, here shown at the position of the H II region complex IC 4701. In this case three narrow lines are visible at velocities of  $-890$ ,  $4465$  and  $9690 \text{ km s}^{-1}$ . The Galactic emission around  $0 \text{ km s}^{-1}$  has mostly been blanked out.

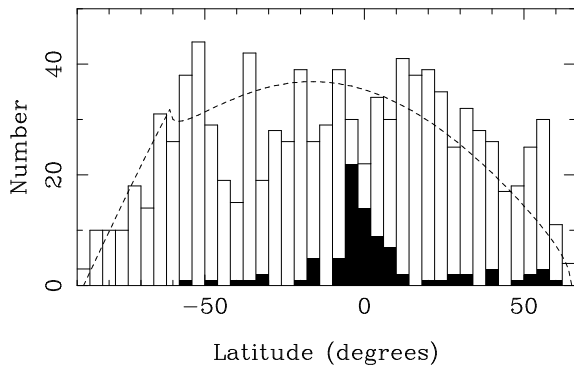


Fig. 12.— Histogram of the Galactic latitudes of all sources in the HIPASS BGC. Newly cataloged galaxies are marked in black. The dotted line shows the relative area of the southern sky covered at each Galactic latitude. Deviations from this line indicate the presence of large-scale structure.

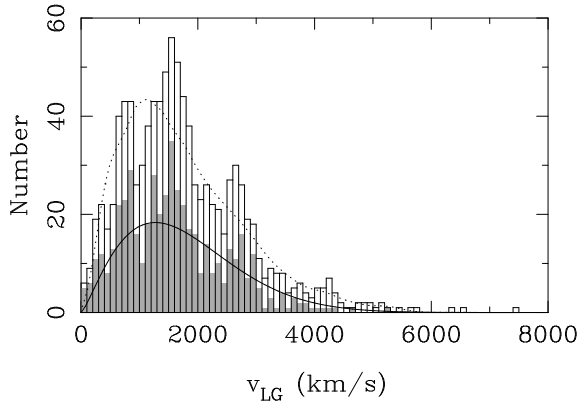


Fig. 13.— Histogram of the HI Local Group velocities,  $v_{\text{LG}}$ , in the HIPASS BGC. We show the full sample of 1000 sources (white) and the complete  $F_{\text{HI}}$ -limited sub-sample (grey) with  $F_{\text{HI}} > 25 \text{ Jy km s}^{-1}$  (see Section 3.7). Overlaid are the selection functions for both samples as derived by Zwaan et al. (2003).

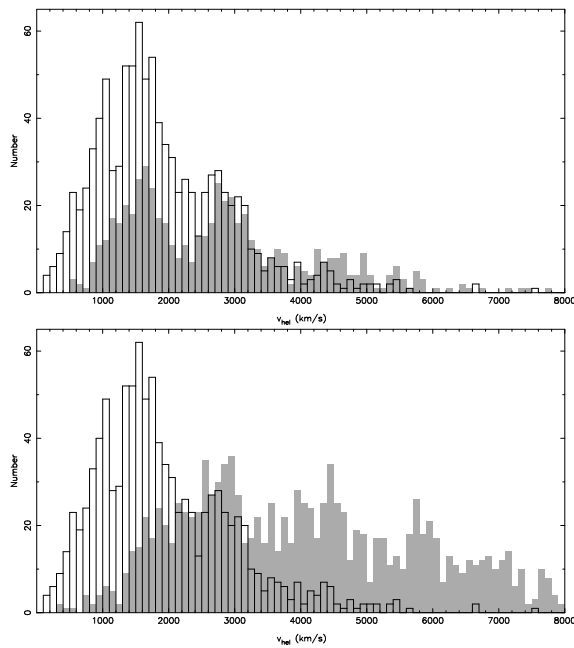


Fig. 14.— Histogram of the HI systemic velocities,  $v_{\text{sys}}$ , of the HIPASS BGC galaxies (white). For comparison we overlaid (in grey) the HI velocity histograms from the targeted samples of Mathewson et al. (1992), top, and Theureau et al. (1998), bottom, selecting only southern galaxies with HI velocities less than  $8000 \text{ km s}^{-1}$ . The samples contain 569 and 1188 galaxies, respectively.

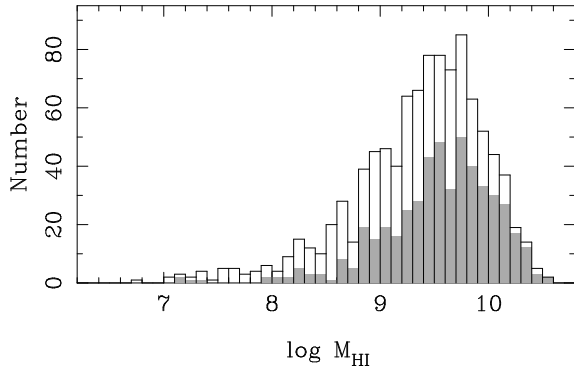


Fig. 15.— Histogram of the HI mass,  $M_{\text{HI}}$ , distribution in the HIPASS BGC. We show the full sample of 1000 sources (white) and the complete  $F_{\text{HI}}$ -limited sub-sample (grey) with  $F_{\text{HI}} > 25 \text{ Jy km s}^{-1}$  (see Section 3.7).

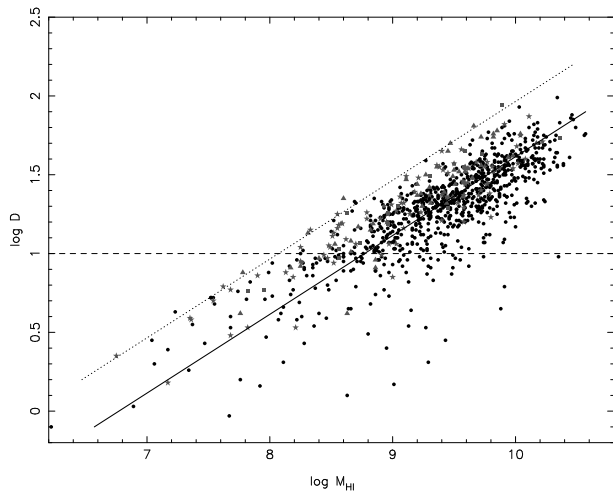


Fig. 16.— Derived distances,  $D$ , of all HIPASS BGC sources against derived HI mass,  $M_{\text{HI}}$ . The solid black line marks the  $F_{\text{HI}}$ -completeness limit ( $F_{\text{HI}} = 25 \text{ Jy km s}^{-1}$ ), while the dotted line denotes the approximate detection limit,  $F_{\text{HI}} = 5 \text{ Jy km s}^{-1}$ , of the BGC. The horizontal dashed line indicates a distance of  $D = 10 \text{ Mpc}$ . Newly cataloged galaxies as well as HI clouds are marked with stars, galaxies with previously unknown velocities with triangles, and galaxies with previously incorrect velocities with squares. In total there are 157 (248) galaxies with  $v_{\text{LG}} < 750 \text{ km s}^{-1}$  ( $1000 \text{ km s}^{-1}$ ) of which 20 (27) are newly cataloged. For comparison see Tully & Fisher (1981a) and Briggs (1997).

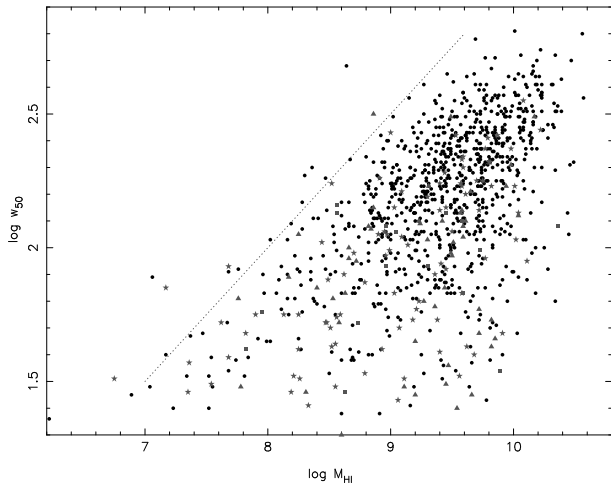


Fig. 17.— Measured velocity width,  $w_{50}$ , of all HIPASS BGC sources against HI mass,  $M_{\text{HI}}$ . While we find a wide range of HI masses for galaxies with narrow line widths (representing mostly low-mass dwarf irregular galaxies and some more massive, nearly face-on spirals), there is a much narrower range for galaxies with large velocity widths (typically massive edge-on spiral galaxies). This trend results from the fact that dwarf irregular galaxies have typically low rotational velocities and masses, both of which gradually increase for type Sd, Sc and Sb galaxies (see Roberts & Haynes 1994). This morphology segregation will be studied in detail in our optical follow-up paper where the inclinations and morphological types of the majority of galaxies in the BGC are available. The dotted line indicates the approximate detection boundary,  $w_{50} \propto M_{\text{HI}}^{0.5}$ , for the BGC. For comparison and an explanation of the symbols see Fig. 16.

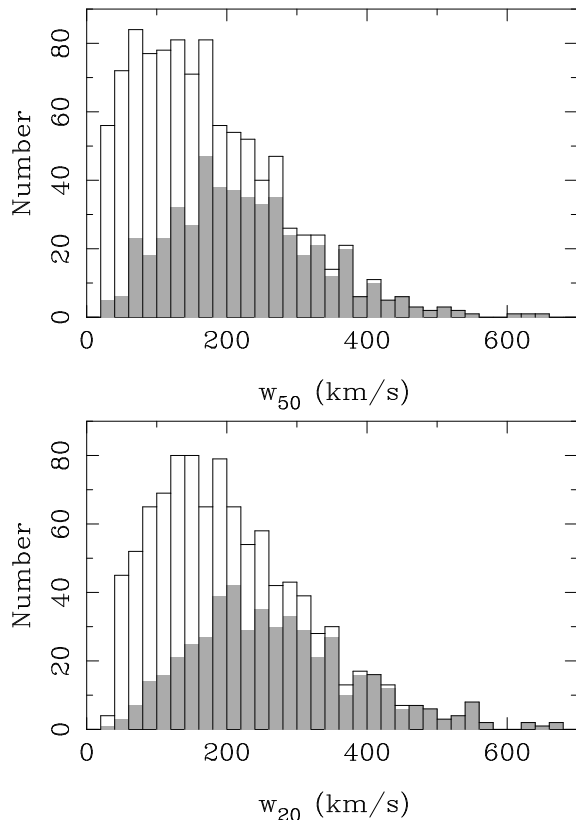


Fig. 18.— Histograms of the measured 50% and 20% H I line widths in the HIPASS BGC. We show the full sample of 1000 sources (white) and the complete  $F_{\text{HI}}$ -limited sub-sample (grey) with  $F_{\text{HI}} > 25 \text{ Jy km s}^{-1}$  (see Section 3.7).

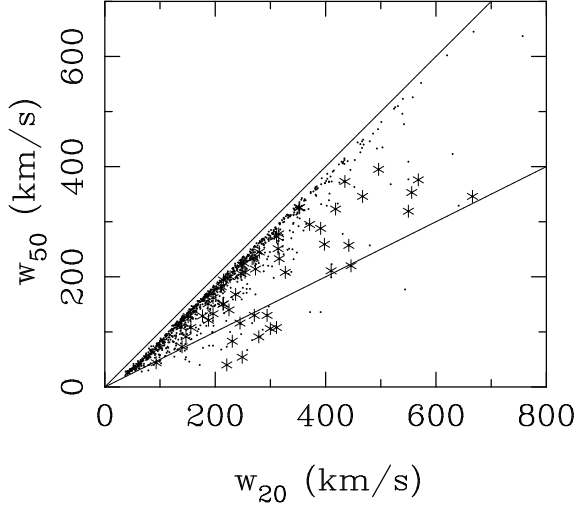


Fig. 19.— A comparison of the 50% and 20% HI velocity line widths. Galaxy pairs and groups, which often show large  $w_{20} / w_{50}$  ratios, are shown as stars. The two lines mark the ratios of 1.0 and 2.0.

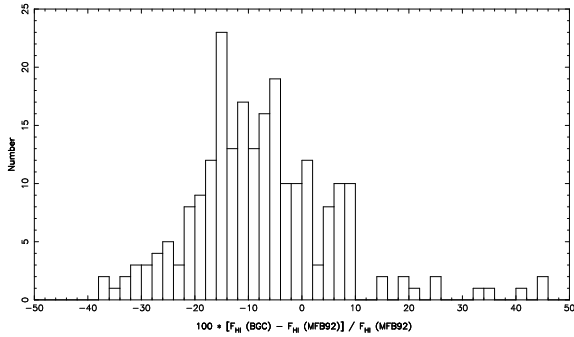


Fig. 20.— Histogram of the percentage difference in HI flux density ( $F_{\text{HI}}$ ) for the 228 galaxies common in the HIPASS BGC and the targeted sample of Mathewson et al. (1992). The median offset from zero is  $-9\%$ , consistent with the difference in absolute flux calibration (see Section 2.1). Not displayed here are 6 galaxies with percentage differences larger than  $50\%$ .

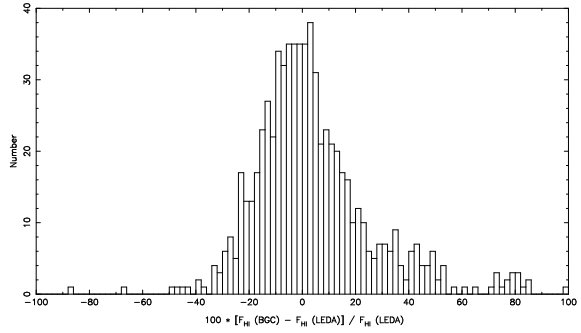


Fig. 21.— Comparison of the integrated HI flux densities,  $F_{\text{HI}}$ , in the HIPASS BGC with those given in LEDA for 692 galaxies (see Section 4.4). Not displayed here are 23 galaxies with percentage differences larger than  $100\%$ .

Fig. 22.— The “HIPASS Bright Galaxy Catalog” contains the 1000 H I-brightest galaxies in the southern sky. Here we show their sky distribution, plus the Magellanic Clouds (unfilled markers), using a zenithal equal area projection of the south celestial hemisphere. Marker size and greyscale represent the integrated H I flux density,  $F_{\text{HI}}$ , and local group velocity,  $v_{\text{LG}}$ , respectively. Galaxies which are  $\times 10$  stronger in  $F_{\text{HI}}$  are displayed  $\times 3$  greater in area. The greyscale ranges from  $v_{\text{LG}} = 0$  (black) to  $4000 \text{ km s}^{-1}$  (white). Only 41 galaxies in the BGC exceed this velocity, with the maximum at  $7413 \text{ km s}^{-1}$ . Nearly 10% of the HIPASS BGC galaxies were previously uncataloged. The most prominent filament across the southern sky is the Supergalactic Plane (SGP), roughly perpendicular to the Galactic Plane. Parallel to the SGP we find at least two further filaments which have previously been described as the toes of a dinosaur’s foot (Lynden-Bell 1994); the toes are clearly connected to the dinosaur’s heel near the Great Attractor (GA). Also prominent is the Local Void ( $v_{\text{LG}} \lesssim 1500 \text{ km s}^{-1}$ ). — The projection is not tangent to the south celestial pole (SCP); its obliquity has instead been chosen so that the supergalactic equator is projected as a straight line. The SCP is marked by a cross just below the center with arms at RA =  $0^{\text{h}}$  (left),  $6^{\text{h}}$  (bottom),  $12^{\text{h}}$ , and  $18^{\text{h}}$ ; the celestial equator on the perimeter is distorted slightly from a circle. Supergalactic and Galactic coordinates are represented by the black and grey graticules, respectively.

Fig. 23.— For comparison with the HIPASS BGC (see Fig. 22) we show the distribution of the 1000 *optically*-brightest galaxies in the southern sky as obtained from LEDA on the basis of their mean apparent total blue magnitudes,  $B_T$ . Marker size has again been set so that galaxies with apparent blue luminosity  $\times 10$  greater are  $\times 3$  larger in area, with the scale factor chosen to make them roughly comparable in size with the HIPASS BGC. Thirty-eight galaxies for which no local group velocity was available in LEDA have been indicated with a cross and white marker. Including these, 163 galaxies exceed  $v_{LG} = 4000 \text{ km s}^{-1}$ . — The HIPASS BGC and our LEDA sample have only  $\sim 400$  galaxies in common. The main differences to Fig. 22 are: (1) the Zone of Avoidance is clearly seen as near horizontal gap in this chart, and (2) galaxies appear more strongly clustered. — The projection, coordinate grids and velocity ranges are the same as in Fig. 22.

Fig. 24.— The HIPASS Bright Galaxy Catalog (left; see also Fig. 22) and the LEDA comparison sample (right; see also Fig. 23) reproduced in discrete velocity ranges (the number of sources in each range is given in brackets): (a)  $v_{\text{LG}} < 1400 \text{ km s}^{-1}$  (BGC + MC: 336 galaxies, LEDA: 244), (b)  $v_{\text{LG}} = 1400 - 2200 \text{ km s}^{-1}$  (BGC: 343, LEDA: 248), and (c)  $v_{\text{LG}} > 2200 \text{ km s}^{-1}$  (BGC: 323, LEDA: 508). Black saturation in (a) is at  $0 \text{ km s}^{-1}$ , and white saturation in (c) is at  $5200 \text{ km s}^{-1}$ . — The projection and coordinate grids are the same as in Figs. 22 and 23.

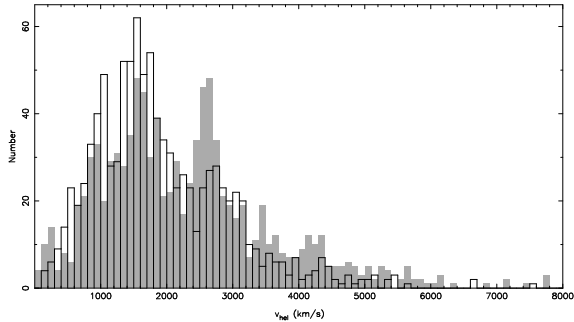


Fig. 25.— Histogram of the H I systemic velocities,  $v_{\text{sys}}$ , of the HIPASS BGC galaxies (white). For comparison we overlaid (in grey) the optical velocity histogram of the 1000 optically brightest galaxies obtained from LEDA (see Section 5).

Fig. 27.— ATCA H I image (contours) of the galaxy ESO376-G022 (HIPASS J1051-34) overlaid onto an optical DSS image (greyscale). The contour levels are 0.5, 1, 2, 3, and 4  $\text{Jy beam}^{-1} \text{ km s}^{-1}$ . The synthesized beam is displayed at the bottom left.

Fig. 28.— Mean H I velocity field in the nearby galaxy NGC 5236 (HIPASS J0317-41) and neighbouring galaxies as obtained from the HIPASS data. The contour levels go from 400 to  $620 \text{ km s}^{-1}$ , in steps of  $20 \text{ km s}^{-1}$ . We measure an integrated H I flux density of  $1630 \text{ Jy km s}^{-1}$ .

Fig. 26.— Distribution of galaxies ( $v < 5000 \text{ km s}^{-1}$ ) in and around the southern Local Void. Galaxies selected from NED (incl. HIZSS galaxies) are marked with open circles, whereas BGC sources are indicated by stars. The newly cataloged galaxies, several of which lie in the Local Void, are easily noted as stars without a surrounding circle. Galactic coordinates are indicated with solid lines (in steps of  $10^\circ$ );  $\alpha, \delta(\text{J2000})$  coordinates are marked with dotted lines.

Table 1: Some parameters of recent blind H I surveys.

H I Survey	Galaxies (new)	Sky area [deg <sup>2</sup> ]	r.m.s. [mJy]	$\delta v$ [km s <sup>-1</sup> ]	velocity range [km s <sup>-1</sup> ]	Ref.
(1)	(2)	(3)	(4)	(5)	(6)	(7)
Arecibo						
– Slice Survey	75 (40)	55	1.7	16	100 to 8340	(1)
– H I Strip Survey (AHISS)	66 (30)	65	0.75	16	–700 to 7400	(2)
– Dual-Beam Survey (ADBS)	265 (81)	430	3.5	32	–650 to 7980	(3)
HIPASS / ZOA						
– Shallow Survey (HIZSS)	110 (67)	1840	15	27	–1200 to 12700	(4)
– South Celestial Cap (SCC)	536 (114)	2414	13	18	–1200 to 12700	(5)
– Bright Galaxy Catalog (BGC)	1000 (91)	20626	13	18	–1200 to 8000	(6)
– HIPASS Catalog (HICAT)	4315	21346	13	18	~300 to 12700	(7)

NOTE.—The BGC selection criteria are given in Section 3.2. Cols. (4) and (5) show the  $1\sigma$  sensitivity and velocity resolution,  $\delta v$ , of each survey.

REFERENCES.—(1) Spitzak & Schneider 1998, (2) Zwaan et al. 1997, (3) Rosenberg & Schneider 2000, (4) Henning et al. 2000, (5) Kilborn et al. 2002, (6) this paper, (7) Meyer et al. (2004).

TABLE 2  
THE HIPASS BRIGHT GALAXY CATALOG

HIPASS Name	RA (J2000)	DEC	$l$	$b$	NED ID	$S_{\text{peak}} \pm \sigma$	$F_{\text{HI}} \pm \sigma$	$v_{\text{sys}} \pm \sigma$	$w_{50}$	$w_{20}$	$v_{\text{LG}}$	$\log M_{\text{HI}}$	flag		
(1)	[hms]	[ $^{\circ}$ $'$ $''$ ]	[ $^{\circ}$ ]	[ $^{\circ}$ ]	(6)	[Jy]	[Jy $\text{km s}^{-1}$ ]	[ $\text{km s}^{-1}$ ]	[ $\text{km s}^{-1}$ ]	[ $\text{km s}^{-1}$ ]	[ $\text{km s}^{-1}$ ]	[ $M_{\odot}$ ]	(17)		
HIPASS J0001-15	00:01:56	-15:28:38	75.8	-73.6	WLM	4.769	0.240	231.8	28.4	-122	2	53	74	-40	7.67*
HIPASS J0002-80	00:02:44	-80:20:48	305.5	-36.5	ESO012-G014	0.255	0.019	23.9	3.1	1958	4	98	130	1762	9.49
HIPASS J0005-28	00:05:38	-28:06:09	24.8	-79.8	ESO409-IG015	0.124	0.014	7.3	1.8	736	7	46	99	758	8.25
HIPASS J0006-41	00:06:18	-41:29:06	332.9	-72.9	ESO293-IG034	0.127	0.018	23.3	4.2	1513	8	236	276	1473	9.33
HIPASS J0008-34	00:08:06	-34:33:31	351.6	-78.1	ESO349-G031	0.166	0.016	5.8	1.6	221	6	30	79	212	7.04
HIPASS J0009-24	00:09:54	-24:57:42	43.7	-80.4	NGC0024	0.340	0.025	50.3	5.1	554	2	210	223	588	8.86
HIPASS J0010-18	00:10:18	-18:15:47	73.9	-77.0	UGCA003	0.304	0.023	7.4	1.9	1545	3	24	41	1610	8.91
HIPASS J0014-23	00:14:01	-23:11:29	55.8	-80.7	NGC0045	1.374	0.071	195.8	14.3	467	2	167	185	507	9.33
HIPASS J0014-70	00:14:11	-69:58:33	307.6	-46.8	ESO050-G006	0.124	0.016	8.6	2.3	4187	5	71	92	4024	9.77
HIPASS J0015-39	00:15:09	-39:13:08	332.7	-75.7	NGC0055	14.595	0.732	1990.2	145.1	129	2	169	197	95	9.01*
HIPASS J0019-22	00:19:07	-22:40:30	62.5	-81.4	MCG-04-02-003	0.191	0.016	16.0	2.5	669	3	119	131	709	8.53
HIPASS J0019-57	00:19:08	-57:38:04	311.3	-59.0	AM0016-575	0.169	0.018	19.8	3.3	1745	4	150	166	1629	9.34
HIPASS J0019-77	00:19:48	-77:06:47	305.2	-39.9	ESO028-G014	0.162	0.017	14.9	2.8	1791	4	114	132	1603	9.21
HIPASS J0022-53	00:22:30	-53:38:55	312.4	-62.9	ESO150-G005	0.143	0.012	13.5	2.0	1436	3	111	125	1335	9.00
HIPASS J0026-33	00:26:36	-33:40:38	340.7	-81.5	NGC0115	0.122	0.017	18.5	3.6	1824	9	200	246	1809	9.41
HIPASS J0030-33	00:30:22	-33:13:41	338.4	-82.4	NGC0134	0.455	0.027	139.5	7.9	1582	3	460	486	1567	10.16
HIPASS J0031-22	00:31:25	-22:45:59	75.7	-83.7	ESO473-G024	0.160	0.016	7.2	1.8	540	4	45	61	572	7.99
HIPASS J0031-10	00:31:30	-10:28:37	106.2	-72.7	MCG-02-02-040	0.127	0.015	31.0	4.1	3573	13	278	431	3659	10.24
HIPASS J0031-05	00:31:43	-05:10:15	110.0	-67.5	NGC0145	0.157	0.016	14.4	2.6	4139	8	78	146	4247	10.04
HIPASS J0033-01	00:33:23	-01:07:45	112.7	-63.6	UGC00328	0.183	0.036	19.4	6.3	1985	7	141	158	2108	9.56
HIPASS J0034-30a	00:34:11	-30:46:00	348.0	-84.8	UGCA006	0.310	0.022	16.9	2.8	1582	3	57	78	1576	9.25
HIPASS J0034-27	00:34:12	-27:48:39	21.8	-86.1	NGC0150	0.220	0.019	46.7	4.6	1584	4	313	342	1592	9.70
HIPASS J0034-08	00:34:48	-08:24:23	110.3	-70.9	NGC0157	0.286	0.019	63.0	4.9	1652	7	209	338	1744	9.91
HIPASS J0035-20	00:35:40	-20:08:51	94.8	-82.1	ESO540-G003	0.118	0.016	20.7	3.6	3292	8	321	360	3333	9.98
HIPASS J0035-25	00:35:45	-25:22:57	58.5	-86.1	IC1558	0.261	0.018	27.7	3.1	1551	3	118	138	1569	9.46
HIPASS J0037-22	00:37:20	-22:37:11	86.8	-84.5	NGC0172	0.151	0.039	22.3	8.0	3048	12	260	287	3077	9.95
HIPASS J0038-46	00:37:43	-46:34:34	310.0	-70.4	ESO242-G020	0.158	0.014	32.9	3.5	3367	12	199	410	3290	10.17
HIPASS J0038-24	00:38:29	-24:17:55	76.3	-85.9	IC1562	0.184	0.018	10.8	2.3	3764	4	50	77	3785	9.81
HIPASS J0039-14a	00:39:04	-14:10:19	109.8	-76.7	NGC0178	0.328	0.020	25.5	3.0	1452	4	71	112	1517	9.39
HIPASS J0040-13	00:40:34	-13:52:25	111.6	-76.5	NGC0210	0.372	0.022	69.6	5.0	1636	3	278	305	1701	9.93
HIPASS J0040-63	00:40:57	-63:27:23	304.9	-53.6	ESO079-G005	0.176	0.020	22.5	3.8	1712	6	153	183	1566	9.36
HIPASS J0042-18	00:42:14	-18:09:44	109.1	-80.8	ESO540-G016	0.138	0.016	17.7	3.0	1553	4	195	212	1598	9.28
HIPASS J0043-22	00:42:59	-22:12:26	101.2	-84.7	IC1574	0.146	0.015	5.4	1.5	363	4	39	55	390	7.54
HIPASS J0046-11	00:46:03	-11:30:14	118.0	-74.3	DDO005	0.187	0.017	16.6	2.7	1622	3	93	111	1694	9.30
HIPASS J0047-20	00:47:06	-20:44:48	113.9	-83.5	NGC0247	3.972	0.201	608.2	42.1	156	2	198	224	187	8.95
HIPASS J0047-25	00:47:31	-25:17:22	97.2	-88.0	NGC0253	3.376	0.173	692.9	42.2	243	2	407	431	254	9.27
HIPASS J0047-09	00:47:45	-09:54:58	119.9	-72.8	UGCA014	0.135	0.016	18.5	3.3	1342	5	144	166	1419	9.19
HIPASS J0047-11	00:47:46	-11:27:14	119.6	-74.3	NGC0255	0.339	0.023	42.8	4.4	1585	4	148	193	1656	9.69
HIPASS J0049-20	00:49:35	-21:01:07	118.9	-83.9	UGCA015	0.144	0.018	3.9	1.5	294	4	25	41	322	7.23
HIPASS J0050-07	00:50:59	-07:03:22	122.6	-69.9	NGC0274/5	0.185	0.014	36.6	3.4	1730	6	233	316	1817	9.70
HIPASS J0051-00	00:51:57	-00:28:21	123.2	-62.4	MCG+00-03-018	0.138	0.016	14.7	2.7	1621	4	169	188	1737	9.27
HIPASS J0052-31	00:52:43	-31:12:17	299.1	-85.9	NGC0289	0.877	0.046	159.1	10.6	1629	2	274	300	1610	10.24
HIPASS J0054-37	00:54:52	-37:40:25	299.2	-79.4	NGC0300	17.078	0.856	1972.6	156.1	146	2	147	166	98	9.29*
HIPASS J0054-07	00:54:57	-07:20:15	125.5	-70.2	NGC0298	0.233	0.017	36.6	3.7	1756	3	209	230	1839	9.72
HIPASS J0056-09	00:56:39	-09:55:33	127.3	-72.8	NGC0309	0.128	0.017	21.1	3.8	5661	7	206	236	5732	10.46
HIPASS J0059-07	00:59:50	-07:35:08	129.1	-70.4	NGC0337	0.248	0.019	51.2	4.6	1648	4	233	272	1726	9.81
HIPASS J0101-07	01:01:34	-07:35:22	130.4	-70.3	NGC0337A	1.231	0.064	98.1	9.7	1074	2	87	106	1151	9.74
HIPASS J0103-03	01:03:01	-03:36:30	130.1	-66.3	MCG-01-03-079	0.122	0.015	8.9	2.2	2587	5	85	103	2679	9.43
HIPASS J0105-06	01:05:01	-06:13:06	132.3	-68.8	MCG-01-03-085	0.475	0.028	62.7	5.5	1096	2	171	189	1176	9.56
HIPASS J0107-69	01:07:30	-69:52:30	300.9	-47.2	NGC0406	0.241	0.018	48.3	4.4	1508	3	240	261	1333	9.56
HIPASS J0109-02	01:09:41	-02:15:52	133.7	-64.8	MCG-01-04-005	0.140	0.016	16.4	2.9	1864	5	149	173	1957	9.42

NOTE.—The full version of this table is in the electronic edition of the Journal.

Table 3: Galaxies for which we adopted independent distances.

Name	NED-ID	$v_{\text{LG}}$ [km s <sup>-1</sup> ]	$\log M_{\text{HI}}$ [M <sub>⊙</sub> ]	$D$ [Mpc]	Reference
(1)	(2)	(3)	(4)	(5)	
HIPASS J0001-15	WLM	-40	7.67	0.925	(1)
HIPASS J0015-39	NGC 0055	95	9.01	1.480	(1)
HIPASS J0054-37	NGC 0300	98	9.29	2.04	(2)
HIPASS J1003-26A	NGC 3109	130	8.63	1.250	(1)
HIPASS J1010-04	Sextans A	113	7.92	1.440	(1)
HIPASS J1929-17	ESO594-G004	24	6.89	1.060	(1)
HIPASS J1944-14	NGC 6822	65	8.16	0.490	(1)
HIPASS J2046-12	DDO 210	3	6.22	0.800	(1)
HIPASS J2202-51	IC 5152	69	7.76	1.590	(1)

NOTE.—Col. (5) lists the adopted independent distances and Col. (6) the corresponding reference. For the LMC and SMC, which are not contained in the HIPASS BGC (see Section 3.2), we adopted distances of 50 and 60 kpc, respectively.

REFERENCES.—(1) Mateo 1998, (2) Willick & Batra 2001.

Table 4: H I properties of the definite H I clouds in the HIPASS BGC.

Name	NED-ID(s) + flag	$S_{\text{peak}}$ [Jy]	$F_{\text{HI}}$ [Jy km s <sup>-1</sup> ]	$v_{\text{sys}}$	$w_{50}$ [km s <sup>-1</sup> ]	$w_{20}$	$v_{\text{LG}}$	$\log M_{\text{HI}}$ [M <sub>⊙</sub> ]
(1)	(2)	(3)	(4)	(5)	(6)	(7)	(8)	(9)
HIPASS J0731-69	new	0.119	14.9	1469	116	267	1195	8.95
HIPASS J1616-55	new (e)	0.455	23.7	409	48	100	256	(7.82) <sup>+</sup>
HIPASS J1712-64	new	0.193	6.2	455	29	49	295	(7.35) <sup>+</sup>
HIPASS J1718-59	new (e)	1.688	58.2	396	33	51	256	(8.21) <sup>+</sup>

NOTE.—<sup>+</sup>If these sources are Magellanic debris, as suggested, then the adopted distances ( $D = v_{\text{LG}}/H_0$ ) and resulting H I masses are incorrect. Assuming  $D = 50$  kpc we obtain H I masses of  $\sim 10^5 M_{\odot}$ .

Table 5: H I properties for the extended sources in the HIPASS BGC; these are flagged with "e" in Table 2.

Name	NED-ID(s)	$F_{\text{HI}}$ [Jy km s <sup>-1</sup> ]	$v_{\text{sys}}$ [km s <sup>-1</sup> ]	log $M_{\text{HI}}$ [M <sub>⊙</sub> ]	Deconvolved Gaussian		$PA$ [deg]
					H I diameter		
(1)	(2)	(3)	(4)	(5)	[arcmin]	[kpc]	(8)
HIPASS J0015–39	NGC 0055	1990.2	129	9.01*	23.2 × 4.9	10 × 2	-71.4
HIPASS J0047–20	NGC 0247	608.2	156	8.95	14.4	10	-10.1
HIPASS J0047–25	NGC 0253	692.9	243	9.27	15.6	15	47.3
HIPASS J0054–37	NGC 0300	1972.6	146	9.29*	27.9 × 18.0	17 × 11	-48.9
HIPASS J0317–41	NGC 1291	90.2	838	9.25	12.9 × 10.9	34 × 29	87.7
HIPASS J0317–66	NGC 1313	462.7	470	9.12	10.1	10	20.0
HIPASS J0403–43	NGC 1512/0	259.3	898	9.74	17.4 × 10.7	48 × 30	59.4
HIPASS J0409–56	NGC 1533	67.6	785	8.97	12.6 × 2.4	28 × 5	-47.8
HIPASS J0411–32	NGC 1532 (c)	248.8	1037	9.90	10.9	37	36.6
HIPASS J0926–76	NGC 2915	108.4	468	8.28	9.0	7	-63.5
HIPASS J1003–26A	NGC 3109	1147.9	403	8.63*	22.7 × 6.2	8 × 2	83.4
HIPASS J1118–32	NGC 3621	884.3	730	9.91	19.0 × 3.6	34 × 7	-9.4
HIPASS J1305–49	NGC 4945	319.1	563	9.15	20.2 × 2.5	25 × 3	47.9
HIPASS J1324–42	NGC 5128 (r)	91.8 <sup>a</sup>	556	8.64 <sup>a</sup>	44.9 × 21.0	59 × 28	28.8
HIPASS J1337–29	NGC 5236 (c)	1630.3	513	9.88	31.2 × 21.4	40 × 28	6.0
HIPASS J1413–65	Circinus	1450.5	434	9.43	33.3 × 19.8	27 × 16	31.2
HIPASS J1532–56	new	64.2	1363	9.58	28.4 × 18.2	131 × 84	-89.3
HIPASS J1616–55	new	23.7	409	(7.82) <sup>+</sup>	58.5 × 26.3	(58 × 26) <sup>+</sup>	41.6
HIPASS J1718–59	new	58.2	396	(8.21) <sup>+</sup>	74.4 × 26.0	(74 × 26) <sup>+</sup>	-88.1
HIPASS J1909–63a	NGC 6744	1031.0	841	10.35	19.3 × 14.7	54 × 41	2.5
HIPASS J1943–06	MCG-01-50-001/2	44.8	1515	9.72	26.3	170	63.3
HIPASS J1944–14	NGC 6822	2524.6	-57	8.16*	39.7 × 13.9	6 × 2	-54.3
HIPASS J2318–42	NGC 7582/90/99	96.8	1571	9.99	17.9	107	67.1
HIPASS J2357–32	NGC 7793	278.5	227	8.80	7.6 × 3.3	7 × 3	-59.1

NOTE.—\* The star after log  $M_{\text{HI}}$  in Col. (5) marks galaxies for which we adopted independent distances (see Table 3).

—<sup>+</sup> If these sources are Magellanic debris, as suggested, then the adopted distances ( $D = v_{\text{LG}}/H_0$ ) and resulting H I masses and diameters are incorrect. Assuming  $D = 50$  kpc we obtain H I masses of  $\sim 10^5 M_{\odot}$  and H I diameters less than 1 kpc.

—<sup>a</sup> A Gaussian fit to the extended H I emission in NGC 5128 results in  $F_{\text{HI}} = 186$  Jy km s<sup>-1</sup> (see Section 3.6).

Table 6: Nearby large-scale structures, clusters and galaxy groups as discussed in Section 5.

Group Name	Alternate Name	$\alpha, \delta$ (J2000) [ <sup>h</sup> m, °]	$l, b$ [°, °]	velocity [km s <sup>-1</sup> ]	Comments
Fornax Wall					
NGC 1672	LGG 119	04 45, -59	269, -39	900–1200	Dorado Cloud
NGC 1566	LGG 114	04 20, -55	264, -43	”	”
NGC 1433	LGG 102/6	03 40, -47	256, -51	”	”
NGC 1399	LGG 096	03 40, -36	237, -54	1300	Fornax Cluster
NGC 1332	LGG 097	03 24, -22	213, -55	1800	Eridanus Cloud
Puppis filament					
Antlia G1	new	09 50, -30	262, 18	900	Antlia Cluster
Antlia G2	new	10 40, -37	276, 19	”	”
		13 30, -30	313, 32		SGP crossing
		12 30, -05	293, 57	1100	Southern Virgo Extension
NGC 4038	LGG 263	12 00, -20	287, 42	1750	Crater Cloud
NGC 5084	LGG 345	13 20, -21	312, 41	1750	”
SGP, Centaurus Wall					
A 3742		21 00, -47	353, -42	4900	Indus Cluster
IC 4765	LGG 422	18 50, -63	332, -24	4500	Pavo Cluster
IC 3370	LGG 298	12 50, -40	303, 20	3000	Centaurus Cluster
A 1060		10 40, -27	270, 27	3800	Hydra Cluster
NGC 3258	LGG 196	10 30, -35	273, 19	2800	Antlia Cluster
Puppis G2	new	07 50, -35	250, -04	2800	Puppis Cluster

Table 7: H I properties of HIPASS BGC galaxies with potentially incorrect (optical) velocities in NED (at the time of the optical identification); for further details see Appendix A. These galaxies are flagged with "w" in Table 2.

Name	HIPASS $v_{\text{sys}}$ [km s <sup>-1</sup> ]	NED-ID	$v_{\text{opt}}$ [km s <sup>-1</sup> ]	Ref.	$v_{\text{HI}}$ [km s <sup>-1</sup> ]	Ref.
(1)	(2)	(3)	(4)	(5)	(6)	(7)
HIPASS J0312-21	6614	ESO547-G019	15711±56	(1)		
HIPASS J0340-45	1547	IC 1986 <sup>a</sup>	1554±35	(2)	1566	(17)
			1274±30	(3)		
			1451±50	(1)		
HIPASS J0341-01	3421	[ISI96] 0339-0209	8459±275	(4)		
HIPASS J0457-42	657	ESO252-IG001	3220	(5)		
			3430	(6)		
			3501±63	(7)		
HIPASS J0732-77	1632	ESO017-G002 <sup>b</sup>	1380±200	(8)		
HIPASS J1043-47	1095	ESO264-G035 <sup>c</sup>	770±60	(9)		
HIPASS J1047-38	711	ESO318-G013 <sup>d</sup>	17±19	(7)		
			17±26	(10)		
HIPASS J1051-34	972	ESO376-G022	1364±53	(7)	972±2	(18)
			1410±90	(11)		
HIPASS J1231-55	1717	ESO172-G004	3939±150	(12)		
HIPASS J1319-33	1683	ESO382-G040	1587±50	(13)	1682	(19)
			13800?	(9)		
HIPASS J1329-55	2573	ESO173-G016 <sup>e</sup>	3608±50	(13)		
HIPASS J1344-47	1386	ESO270-G028	3410±70	(14)		
HIPASS J1350-48b	4253	ESO221-G006	4510±100	(9)	4013	(20)
			4285±50	(13)		
			4400	(6)		
HIPASS J1657-60	1035	ESO138-G009	—	—	881	(20)
HIPASS J1832-57	2746	ESO140-G023	2698±50	(13)	2730±2	(17)
			4800±5	(15)		
HIPASS J2257-02	3009	PGC070104 <sup>f</sup>	2770±275	(4)		
			4605±10	(16)		

NOTE.— <sup>a</sup> The optical velocities listed for IC 1986 are likely to be from different parts of this irregular galaxy. <sup>b</sup> The face-on appearance of the Sa galaxy ESO017-G002 agrees with its narrow H I profile ( $w_{50} = 29$  km s<sup>-1</sup>). <sup>c</sup> There is an uncataloged neighbour galaxy  $\sim 4'$  SW of ESO264-G035. <sup>d</sup> The ATCA H I image of ESO318-G013 shows a rather asymmetric H I distribution, centered on the western part of the galaxy. The HIPASS H I profile is very narrow ( $w_{50} = 42$  km s<sup>-1</sup>) for what appears to be a peculiar, nearly edge-on galaxy. <sup>e</sup> ESO173-G016 is a spiral galaxy with an extended low-surface brightness disk, barely visible in the DSS 1 and 2. <sup>f</sup> Bothun et al. (1993) refer to a preprint by Impey and collaborators. Note that Impey et al. (1996; ISI96) list two LSB galaxies: 2254(36)-0245 ( $v_{\text{opt}} = 2770$  km s<sup>-1</sup>) and 2254(58)-0246 ( $v_{\text{opt}} = 4606$  km s<sup>-1</sup>).

REFERENCES.—(1) Da Costa et al. 1991, (2) Peterson et al. 1986, (3) Lauberts et al. 1989 (ESO-LV), (4) Impey et al. 1996 (ISI96), (5) Lauberts & Valentijn 1989, (6) Fairall & Jones 1991, (7) de Vaucouleurs et al. 1991 (RC3), (8) Fairall 1980, (9) Fairall et al. 1989, (10) Hopp & Materne (1985), (11) Penston et al. 1977, (12) Fairall et al. 1998, (13) Dressler 1991, (14) Visvanathan & Yamada 1996, (15) Peterson 1986, (16) Bothun et al. (1993), (17) Tully 1988 (Nearby Galaxy Catalog), (18) Fouqué et al. 1990, (19) Coté et al. 1997, (20) Huchtmeier & Richter 1989.

This figure "Koribalski.fig1.panel01.jpg" is available in "jpg" format from:

<http://arxiv.org/ps/astro-ph/0404436v1>

This figure "Koribalski.fig1.panel02.jpg" is available in "jpg" format from:

<http://arxiv.org/ps/astro-ph/0404436v1>

This figure "Koribalski.fig11.jpg" is available in "jpg" format from:

<http://arxiv.org/ps/astro-ph/0404436v1>

This figure "Koribalski.fig22.jpg" is available in "jpg" format from:

<http://arxiv.org/ps/astro-ph/0404436v1>

This figure "Koribalski.fig23.jpg" is available in "jpg" format from:

<http://arxiv.org/ps/astro-ph/0404436v1>

This figure "Koribalski.fig24a.jpg" is available in "jpg" format from:

<http://arxiv.org/ps/astro-ph/0404436v1>

This figure "Koribalski.fig24b.jpg" is available in "jpg" format from:

<http://arxiv.org/ps/astro-ph/0404436v1>

This figure "Koribalski.fig24c.jpg" is available in "jpg" format from:

<http://arxiv.org/ps/astro-ph/0404436v1>

This figure "Koribalski.fig24d.jpg" is available in "jpg" format from:

<http://arxiv.org/ps/astro-ph/0404436v1>

This figure "Koribalski.fig24e.jpg" is available in "jpg" format from:

<http://arxiv.org/ps/astro-ph/0404436v1>

This figure "Koribalski.fig24f.jpg" is available in "jpg" format from:

<http://arxiv.org/ps/astro-ph/0404436v1>